Available online at www.sciencedirect.com
ScienceDirect
Geochimica et Cosmochimica Acta 74 (2010) 5349–5367
Geochimica et Cosmochimica Acta
www.elsevier.com/locate/gca

Joint determination of ^{40}K decay constants and $^{40}Ar^*/^{40}K$ for the Fish Canyon sanidine standard, and improved accuracy for $^{40}Ar/^{39}Ar$ geochronology

Paul R. Renne [a,b,*], Roland Mundil [a], Greg Balco [a,b], Kyoungwon Min [c], Kenneth R. Ludwig [a]

[a] Berkeley Geochronology Center, 2455 Ridge Rd., Berkeley, CA 94709, USA
[b] Department of Earth and Planetary Science, University of California, Berkeley, CA 94720, USA
[c] Department of Geological Sciences, University of Florida, 241 Williamson Hall, Gainesville, FL 32611, USA

Received 1 April 2010; accepted in revised form 11 June 2010; available online 25 June 2010

Abstract

$^{40}Ar/^{39}Ar$ and K–Ar geochronology have long suffered from large systematic errors arising from imprecise K and Ar isotopic data for standards and imprecisely determined decay constants for the branched decay of ^{40}K by electron capture and β^- emission. This study presents a statistical optimization approach allowing constraints from ^{40}K activity data, K–Ar isotopic data, and pairs of ^{238}U–^{206}Pb and $^{40}Ar/^{39}Ar$ data for rigorously selected rocks to be used as inputs for estimating the partial decay constants (λ_ε and λ_β) of ^{40}K and the $^{40}Ar^*/^{40}K$ ratio (κ_{FCs}) of the widely used Fish Canyon sanidine (FCs) standard. This yields values of $\kappa_{FCs} = (1.6418 \pm 0.0045) \times 10^{-3}$, $\lambda_\varepsilon = (0.5755 \pm 0.0016) \times 10^{-10}\ a^{-1}$ and $\lambda_\beta = (4.9737 \pm 0.0093) \times 10^{-10}\ a^{-1}$. These results improve uncertainties in the decay constants by a factor of >4 relative to values derived from activity data alone. Uncertainties in these variables determined by our approach are moderately to highly correlated ($\mathrm{cov}(\kappa_{FCs}, \lambda_\varepsilon) = 7.1889 \times 10^{-19}$, $\mathrm{cov}(\kappa_{FCs}, \lambda_\beta) = -7.1390 \times 10^{-19}$, $\mathrm{cov}(\lambda_\varepsilon, \lambda_\beta) = -3.4497 \times 10^{-26}$) and one must take account of the covariances in error propagation by either linear or Monte Carlo methods. $^{40}Ar/^{39}Ar$ age errors estimated from these results are significantly reduced relative to previous calibrations. Also, age errors are smaller for a comparable level of isotopic measurement precision than those produced by the $^{238}U/^{206}Pb$ system, because the $^{40}Ar/^{39}Ar$ system is now jointly calibrated by both the ^{40}K and ^{238}U decay constants, and because $\lambda_\varepsilon(^{40}K) < \lambda(^{238}U)$. Based on this new calibration, the age of the widely used Fish Canyon sanidine standard is 28.305 ± 0.036 Ma. The increased accuracy of $^{40}Ar/^{39}Ar$ ages is now adequate to provide meaningful validation of high-precision U/Pb or astronomical tuning ages in cases where closed system behavior of K and Ar can be established.

1. INTRODUCTION

The $^{40}Ar/^{39}Ar$ dating method is one of the most important means of measuring geologic time over most of Earth's history. In addition to its wide age range of applicability and the existence of internal reliability criteria, this technique is of great importance because it is capable of exemplary precision, better than 0.1%[1] of the age in many cases, which is attainable by only the U/Pb method among widely used geochronometers. The $^{40}Ar/^{39}Ar$ method is especially important in the Cenozoic Era (the past 66 million years), and most currently used Cenozoic time scales (e.g., Cande

* Corresponding author at: Berkeley Geochronology Center, 2455 Ridge Rd., Berkeley, CA 94709, USA. Tel.: +1 510 644 1350; fax: +1 510 644 9201.
E-mail address: prenne@bgc.org (P.R. Renne).

[1] All uncertainties herein are expressed at the level of one standard deviation or 68% confidence.

0016-7037/$ - see front matter © 2010 Elsevier Ltd. All rights reserved.
doi:10.1016/j.gca.2010.06.017

and Kent, 1995; Aguilar et al., 1996; Gradstein et al., 2004) are calibrated almost exclusively by this method whereas U–Pb data are favored in the pre-Mesozoic. $^{40}Ar/^{39}Ar$ dating has been employed over the widest temporal range of any dating method, having illuminated important questions in geology, cosmology, archeology, and paleontology through the age of emplacement (i.e., volcanic) or cooling (i.e., plutonic and metamorphic) of rocks.

$^{40}Ar/^{39}Ar$ dating is based on the ^{40}K–^{40}Ar method, which requires knowledge of the decay constants both for the $^{40}K \rightarrow {}^{40}Ar$ electron capture decay (λ_ε) and the $^{40}K \rightarrow {}^{40}Ca$ β^- decay (λ_β). A β^+ decay mode was inferred by Beckinsale and Gale (1969) to account for 0.001% of ^{40}K activity, and has subsequently been ignored by other workers – this decay mode has never been detected to our knowledge. The $^{40}Ar/^{39}Ar$ method requires, in addition, the use of natural standards with either accurately-known $^{40}Ar/^{40}K$ ratios or independent knowledge of the age. The ^{40}K decay constants in widespread use since 1977 (Steiger and Jäger, 1977) are derived from a compilation of ^{40}K activity data (Beckinsale and Gale, 1969) combined with a revised value for the isotopic abundance of ^{40}K (Garner et al., 1975). Following the suggestion of Steiger and Jäger (1977) the IUGS Subcommission on Geochronology adopted a value for λ_{tot} ($= \lambda_\varepsilon + \lambda_\beta$) of 5.543×10^{-10} a^{-1} with a branching ratio of 0.1171 for $\lambda_\varepsilon/\lambda_\beta$, but did not consider the uncertainties in these values. Despite its excellent potential age resolution the $^{40}Ar/^{39}Ar$ method as calibrated by these constants is limited in accuracy to no better than 2% arising mainly from the propagation of systematic errors in the ^{40}K decay constants and the ^{40}K–^{40}Ar data for standards (Min et al., 2000).

Efforts to improve the accuracy of $^{40}Ar/^{39}Ar$ dating have focused on refining the ages of standards such as the widely used Fish Canyon sanidine (FCs), whose age has been addressed by the following approaches individually or in combination: (i) intercalibration with "first principles" standards (for which K–Ar data were available, e.g., Hurford and Hammerschmidt, 1985; Renne et al. 1998; Lanphere and Dalrymple, 2000; Spell and McDougall, 2003); (ii) comparison with ages based on orbital tuning (Renne et al., 1994; Hilgen et al., 1997; Kuiper et al., 2008); and (iii) comparison with results from coexisting mineral phases and/or different radioisotopic systems (e.g., Baksi et al., 1996; Villeneuve et al., 2000; Lanphere and Baadsgaard, 2001; Schmitz and Bowring, 2001; Bachman et al., 2007). The references cited above are intended to be indicative rather than exhaustive; for a more complete enumeration of data relevant to the age of FCs the reader is encouraged to consult those sources as well as the summary by Dazé et al. (2003).

The results of the various efforts to determine the age of FCs vary by several percent, far beyond what is expected from typical reported precision. Consensus is lacking as to the cause of this dispersion, but it certainly includes systematic errors and inconsistent interlaboratory calibrations as well as real geologic differences between the ages measured by different radioisotopic systems on different materials. Overall, the trend has been that older ages for FCs have been accepted in more recent times, culminating with the unprecedentedly precise age of 28.201 ± 0.023 Ma reported by Kuiper et al. (2008) based on orbital tuning. The result of Kuiper et al. (2008) represented a significant advance in reconciling $^{40}Ar/^{39}Ar$ ages with those based on other chronometers including orbital tuning, and has achieved wide acceptance.

Despite the progress in determining the ages of standards presented by Kuiper et al. (2008), little progress has been made in refining the ^{40}K decay constants since the synthesis of Beckinsale and Gale (1969), updated by Steiger and Jäger (1977). As is discussed in the following, knowledge of the age of a standard in and of itself is only a partial solution to calibrating the $^{40}Ar/^{39}Ar$ system because miscalibrated decay constants accrue error as measured isotopic data are extrapolated to samples whose ages differ from that of the standard. Moreover, if we accept the K–Ar isotopic data for $^{40}Ar/^{39}Ar$ standards (i.e., as summarized by Jourdan and Renne, 2007), the only way to reconcile these data with the orbitally tuned result of Kuiper et al. (2008) is to adjust either or both of the principal ^{40}K decay constants.

Min et al. (2000) and Kwon et al. (2002) observed that one could improve the accuracy of determination of both λ_{tot} and the age of the FCs standard (or, in principle, any other standard) by comparing the $^{40}Ar/^{39}Ar$ ages of volcanic rocks with ages determined for the same samples by independent methods, in most cases by the U–Pb method. The U decay constants, particularly that for ^{238}U, are significantly more precisely known than λ_{tot} or the age of FCs, so one can estimate these latter two quantities by finding values for them that best reconcile $^{40}Ar/^{39}Ar$ and ^{238}U–^{206}Pb* ages, as follows.

The $^{40}Ar^*/^{39}Ar_K$ isotope ratio of a neutron-irradiated sample is related to these two parameters and to the true age of the sample by:

$$t_{std} = \frac{1}{\lambda_{tot}} \ln\left[\frac{(e^{\lambda_{tot}\tau_i} - 1)}{R_i} + 1\right] \quad (1)$$

where λ_{tot} is the total ^{40}K decay constant, τ_i is an independently determined age of sample i, and R_i embodies the relationship between sample i and the standard, defined (Renne et al., 1998) by:

$$R_i \equiv \frac{(^{40}Ar^*/^{39}Ar_K)_i}{(^{40}Ar^*/^{39}Ar_K)_{std}} \equiv \frac{(e^{\lambda_{tot} t_i} - 1)}{(e^{\lambda_{tot} t_{std}} - 1)} \quad (2)$$

where $^{40}Ar^*$ denotes radiogenic ^{40}Ar and $^{39}Ar_K$ indicates ^{39}Ar produced from K by neutron irradiation. A U–Pb age (or other independent determination of the true age) and measurement of R_i for a particular sample thus define a relation between t_{std} and λ_{tot}. Kwon et al. (2002) considered five such pairs and applied a maximum likelihood method (discussed in more detail later) to find values of t_{std} and λ_{tot} that best fit these observations. Graphically, this can be thought of as determining the mutual intersection of a number of curves defined by Eq. (1) for (τ_i, R_i) pairs.

The approach of Kwon et al. (2002) showed the effectiveness of the basic idea of employing independently dated samples to calibrate the $^{40}Ar/^{39}Ar$ system, but did not incorporate constraints from activity measurements or isotopic data for the standard. In this work, these constraints

Table 1
Independent parameter estimates used in the regression. See Sections 2.1–2.4 for discussion.

Parameter	Value	Uncertainty (σ)	Relative Unc. (%)	Ref.
κ_{FCs}	1.6408×10^{-3}	0.0047×10^{-3}	0.289	This work
λ_ε	0.580×10^{-10} a^{-1}	0.007×10^{-10} a^{-1}	1.207	Min et al. (2000)
λ_β	4.884×10^{-10} a^{-1}	0.049×10^{-10} a^{-1}	1.003	Min et al. (2000)
λ_{tot}	5.5545×10^{-10} a^{-1}	0.0109×10^{-10} a^{-1}	0.196	This work

are incorporated to determine t_{std} and both decay constants for ^{40}K. These parameters are related to (τ_i, R_i) pairs according to:

$$\kappa_{std} \equiv \left(\frac{^{40}Ar^*}{^{40}K}\right)_{std} = \left(\frac{\lambda_\varepsilon}{\lambda_\varepsilon + \lambda_\beta}\right)\frac{\left[e^{(\lambda_\varepsilon+\lambda_\beta)\tau_i} - 1\right]}{R_i} \quad (3)$$

in which Eq. (1) is transformed into a function of κ_{std}, the true (dimensionless) ^{40}Ar*/^{40}K ratio of the standard, rather than t_{std}. The (τ_i, R_i) pairs define relations between λ_ε, λ_β, and κ analogous to their relationship to t_{std} and λ_{tot} as employed by Kwon et al. (2002). We use a least-squares solution method similar to that of Kwon et al. (2002) to find values of λ_ε, λ_β, and κ that best fit (i) a set of such relations defined by seventeen (τ_i, R_i) pairs and (ii) independent determinations of λ_ε, λ_β, λ_{tot}, and κ_{std}. Graphically, this can be thought of as determining the mutual intersection of curved surfaces defined by Eq. (3) for the (τ_i, R_i) pairs, and planes defined by the independent measurements of λ_ε, λ_β, and κ. We show that the estimates of λ_ε, λ_β, and κ_{std} derived from this exercise (i) successfully reconcile U–Pb and ^{40}Ar/^{39}Ar ages for our entire data set, (ii) are significantly more precise than those determined from the existing independent measurements alone, and (iii) yield ^{40}Ar/^{39}Ar dates of unprecedented accuracy.

2. SUMMARY OF EXISTING DATA

A summary of existing constraints on λ_ε, λ_β, λ_{tot}, and the value of κ for the Fish Canyon sanidine (κ_{FCs}), are given in Table 1 and discussed below.

2.1. ^{40}Ar/^{40}K measurements of FCs

Three sources of data are available for the ^{40}Ar*/^{40}K ratio (κ_{FCs} value) of sanidine from the Fish Canyon Tuff. Steven et al. (1967) and Hurford and Hammerschmidt (1985) reported K–Ar data yielding mean ages of 27.9 ± 0.4 and 27.99 ± 0.27 Ma (respectively) based on measurements of ^{40}Ar concentration by isotope dilution, K concentration by flame photometry, and the constants of Steiger and Jäger (1977). These K–Ar ages correspond to κ_{FCs} values of $(1.634 \pm 0.023) \times 10^{-3}$ and $(1.639 \pm 0.016) \times 10^{-3}$. Jourdan and Renne (2007) calibrated FCs against four primary standards (NL-25, Hb3gr, GHC-305, and GA1550) whose ^{40}K and ^{40}Ar were determined by isotope dilution using independently calibrated tracers. Equivalent K–Ar ages for FCs referred to these primary standards are 28.43 ± 0.40, 28.03 ± 0.17, 27.99 ± 0.13, and 28.03 ± 0.16 Ma (respectively) yielding κ_{FCs} values of $(1.665 \pm 0.023) \times 10^{-3}$, $(1.641 \pm 0.010) \times 10^{-3}$, $(1.639 \pm 0.008) \times 10^{-3}$, and $(1.641 \pm 0.009) \times 10^{-3}$. The weighted mean κ_{FCs} value from all six of these independent K–Ar or K–Ar equivalent measurements is $(1.6408 \pm 0.0047) \times 10^{-3}$, with an MSWD[2] of 0.25 and probability-of-fit of 0.94. Thus we conclude that the between-measurement scatter is consistent with stated uncertainties, and that the stated uncertainties may be overestimated.

2.2. β Activity data

Available data for the β activity of ^{40}K were evaluated by Min et al. (2000), who concluded that the previous compilation by Beckinsale and Gale (1969), which served as the basis for the decay constants recommended by Steiger and Jäger (1977), was flawed by arbitrary selection of activity data and, to a lesser extent, outdated physical constants. Using the more objective compilation of Endt and Van der Leun (1973), and updating the values of Avogadro's number and the atomic weight of K, Min et al. (2000) calculated a value of $(4.884 \pm 0.049) \times 10^{-10}$ a^{-1} for λ_β, which is used herein.

2.3. Electron capture activity data

Activity-based estimates of λ_ε are based on measurements of 1.46 MeV γ radiation. As with the β activity data, Min et al. (2000) used the compilation of Endt and Van der Leun (1973) and updated the values of physical constants to obtain a value of $\lambda_\varepsilon = (0.580 \pm 0.007) \times 10^{-10}$ a^{-1}. A hypothetical electron capture decay direct to ground state (without γ emission), accounting for 0.16% of total ^{40}K decay, was incorporated by Beckinsale and Gale (1969) and subsequently (implicitly) by Steiger and Jäger (1977). Lacking any evidence for the existence of this decay mode, we follow Min et al. (2000) in excluding it from consideration.

2.4. Liquid scintillation activity data

Two recent measurements of the total ^{40}K activity determined by liquid scintillation counting (LSC) techniques are available. Grau Malonda and Grau Carles (2002) measured solutions of KNO_3 with natural K, and reported a λ_{tot} value of $(5.554 \pm 0.009) \times 10^{-10}$ a^{-1}. Kossert and Günther (2004) measured solutions of KNO_3 and KCl with natural K, and reported an identical value of $(5.554 \pm 0.013) \times 10^{-10}$ a^{-1}. Combining all of the specific activities reported in these two studies with stoichiometric K concentrations yields a mean activity per atom of K of $(2.05445 \pm 0.00162) \times 10^{-21}$ Bq/[K] (mean ± standard error of the

[2] Mean square of weighted deviates (McIntyre et al., 1966).

mean), which then allows propagating the uncertainty in $^{40}K/K$ ($(1.1672 \pm 0.0021) \times 10^{-4}$; Garner et al., 1975) as a systematic error. Thus, we obtain a value of $\lambda_{tot} = (5.5545 \pm 0.0109) \times 10^{-10}\ a^{-1}$ using the expression and constants (Avogadro's number, atomic weight of K, and seconds per tropical year) used by Min et al. (2000).

2.5. $^{206}Pb/^{238}U$–$^{40}Ar/^{39}Ar$ data pairs

The α activity measurements of ^{238}U by Jaffey et al. (1971) provided an exceptionally precise value of $\lambda(^{238}U) = (1.55125 \pm 0.00083) \times 10^{-10}\ a^{-1}$; consequently this nuclide has long been considered to present a logical basis for comparison or normalization of other decay constants (e.g., Wetherill et al., 1956; Steiger and Jäger, 1977; Patchett and Tatsumoto, 1980; Luck et al., 1980; Minster et al., 1982; Begemann et al., 2001; Schoene et al., 2006; Mattinson, in press). Note that, as pointed out by Begemann et al. (2001), many of the normalization studies (e.g., Patchett and Tatsumoto, 1980; Luck et al., 1980; Minster et al., 1982) used $^{207}Pb/^{206}Pb$ (rather than $^{206}Pb/^{238}U$) ages as the normalization basis, which involves not only the ^{238}U–^{206}Pb decay, but also (and to a greater degree) that of ^{235}U–^{207}Pb. Thus $^{207}Pb/^{206}Pb$ ages are not only qualitatively different from $^{206}Pb/^{238}U$ ages, but also incur a substantial and generally overlooked penalty from the uncertainties in $\lambda(^{238}U)$ as well as $\lambda(^{235}U)$ (Ludwig, 2000). In this study only $^{206}Pb/^{238}U$ ages are used, as discussed further below.

The validity of our analysis rests in part on the validity of the value and uncertainty of the ^{238}U decay constant reported by Jaffey et al. (1971). We share the conclusion of Schön et al. (2004) that further measurements of comparable precision are desirable in order to meaningfully evaluate the interlaboratory reproducibility of the Jaffey et al. (1971) results. Nonetheless we adopt the value and its uncertainty given by Jaffey et al. (1971). As we show subsequently, when we use these values we find that $^{206}Pb/^{238}U$ ages are consistent at their stated uncertainties with all measurements of λ_ε, λ_β, λ_{tot}, and κ_{FCs}, which tends to validate the decay constant uncertainty of Jaffey et al. (1971). We then use pairs of $^{40}Ar/^{39}Ar$ and $^{206}Pb/^{238}U$ data from individual rocks, whose substitution into Eq. (3) define relations among κ_{FCs}, λ_ε, and λ_β. The data pairs are shown in Table 2. The $^{40}Ar/^{39}Ar$ data are presented as R values relative to the Fish Canyon sanidine standard, as defined in Eq. (2) and based on data summarized in Table 3.

Surprisingly few pairs of reliable $^{206}Pb/^{238}U$ and $^{40}Ar/^{39}Ar$ data exist that permit valid comparison of these systems with temporal resolution approaching the precision of which the two systems are capable. The requirement of effectively simultaneous closure of both the U–Pb and K–Ar systems essentially limits the choices to precisely dated (precision <1%) volcanic products, whereas the vast majority of rocks dated by both methods are of plutonic or metamorphic origin (e.g., Schoene et al., 2006). Moreover, only volcanic materials free from reheating effects, as inferred from $^{40}Ar/^{39}Ar$ age spectrum and petrographic analysis, can be considered reliable. The volcanic origin criterion is particularly important for young (e.g., Phanerozoic) rocks wherein differential closure temperatures (Dodson, 1973) can produce relative age differences of several percent even at the geologically rapid cooling rates (>100 °C/Ma) typical of subvolcanic intrusions. In addition, the effects of pre-eruptive magma residence time of zircons must be considered even in volcanic rocks, so that pre-Mesozoic materials, whose age bias from pre-eruptive zircons should be less than 1‰ (e.g., Simon et al., 2008), are preferred.

Table 2
(τ_i, R_i) pairs used in the regression. See Appendix A1 for explanation and description of samples.

Sample	τ[a] (Ma)	σ_τ (Ma)	σ_τ (%)	Ref.	R[b]	σ_R	σ_R (%)	Ref.
79CE	1.919×10^{-3}			2	6.789×10^{-5}	5.5×10^{-7}	0.81%	2
IP	17.42	0.03	0.17	3	0.60556	0.00249	0.41	3
P1T-2	125.65	0.17	0.14	1	4.5494	0.0061	0.13	4
PR94-7	133.06	0.26	0.20	1	4.8205	0.0153	0.32	1
NMB	201.27	0.13	0.07	5	7.4636	0.0072	0.10	6
MSG-09	242.14	0.45	0.19	7	9.0619	0.0122	0.13	7
SH-10	252.17	0.36	0.14	8	9.4983	0.0102	0.11	1,9
D3T	252.40	0.33	0.13	8	9.4918	0.0041	0.04	9
SH-09	252.60	0.33	0.06	8	9.5102	0.0059	0.06	1
PD97-2	253.02	0.50	0.20	1	9.4958	0.0122	0.13	10
SH-27	253.24	0.33	0.13	8	9.5295	0.0068	0.07	1
SH-16	253.68	0.30	0.12	8	9.5391	0.0085	0.09	1
SH-08	257.30	0.30	0.12	8	9.6987	0.0053	0.05	1
PaV	327.99	0.45	0.14	1	12.6039	0.0148	0.12	1
DK-LQ	454.59	0.56	0.12	1	18.0900	0.0523	0.29	11
F-239	1094.2	1.15	0.11	5	52.9011	0.1162	0.22	12
EGB-032	2067.5	1.4	0.07	5	135.6389	0.1821	0.13	1

Data sources: 1 – This study; 2 – Renne et al. (1998); 3 – Palfy et al. (2007); 4 – Chang et al. (2009); 5 – Schoene et al. (2006); 6 – Jourdan et al. (2009) 7 – Mundil et al. (2010); 8 – Mundil et al. (2004); 9 – Renne et al. (1995); 10 – Renne et al. (2001); 11 – Min et al. (2001); 12 – Min et al. (2000).

[a] τ refers to independent age constraint, which is a calendar age for 79CE, and $^{206}Pb/^{238}U$ ages (uncorrected for residence time) for all others.

[b] R refers to the relationship between $^{40}Ar^*/^{39}Ar_K$ for the sample and that of the FCs standard, as defined by Eq. (2).

Table 3
Summary of new data used to compile *R*-values, based on Ar isotope data reported in EA-2.

Sample	Lab. #	F_{unk}	$\pm\sigma$	F_{std}	$\pm\sigma$	R	$\pm\sigma$	$\pm\sigma$ (%)
PR94-7 Sanidine	30771-01	11.55760	0.00190					
	30771-02	11.55990	0.01200					
	30771-03	11.56650	0.01050					
	30771-04	11.55650	0.01100					
	30771-05	11.55650	0.01130					
	30771-06	11.57490	0.01210					
FCs[a]	21181			2.40589	0.00259			
	21183			2.39648	0.00246			
	21185			2.39079	0.00317			
Summary		11.55820	0.00180	2.39772	0.00763	4.82050	0.01535	0.318
SH-16 Sanidine	33367	28.78470	0.01160					
FCs	33366			3.01755	0.00238			
Summary		28.78470	0.01160	3.01755	0.00238	9.53910	0.00846	0.089
SH-08 Sanidine	33010-11	5.71136	0.00385					
	33010-31	5.71081	0.00372					
	33010-32	5.71196	0.00369					
	33010-33	5.71743	0.00341					
FCs	33010			0.58906	0.00026			
Summary		5.71312	0.00183	0.58906	0.00026	9.69866	0.00532	0.055
SH-27 Sanidine	33016-11	5.56972	0.00733					
	33016-12	5.57344	0.00971					
	33016-13	5.57419	0.00883					
	33016-14	5.57406	0.00772					
	33016-15	5.56742	0.01134					
	33016-17	5.58538	0.00850					
	33016-19	5.56439	0.01201					
	33016-20	5.56634	0.01330					
	33016-22	5.56860	0.01059					
FCs	33017			0.58478	0.00026			
Summary		5.57269	0.00312	0.58478	0.00026	9.52952	0.00680	0.071
SH-10 Plagioclase	33018-21	5.57037	0.02255					
	33018-22	5.58223	0.01006					
	33018-23	5.58423	0.01044					
FCs	33019			0.58743	0.00050			
Summary		5.58199	0.00690	0.58743	0.00050	9.50237	0.01428	
Previous Data ([b])						9.49405	0.01464	
Global Summary						9.49831	0.01022	0.108
SH-09 Sanidine	33020-11	5.59190	0.00337					
	33020-12	5.59870	0.00398					
FCs	33021			0.58813	0.00027			
Summary		5.59318	0.00241	0.58813	0.00027	9.51018	0.00594	0.062
PaV Hornblende	32451-01	37.35305	0.04465					
	32541-02	37.30356	0.05521					
	32541-03	37.19669	0.26240					
	32451-10	37.05151	0.14302					
	32451-13	37.00940	0.15900					
FCs	32452			2.95963	0.00230			
Summary		37.30280	0.03270	2.95963	0.00230	12.60389	0.01475	0.117

(*continued on next page*)

Table 3 (*continued*)

Sample	Lab. #	F_{unk}	$\pm\sigma$	F_{std}	$\pm\sigma$	R	$\pm\sigma$	$\pm\sigma$ (%)
EGB-032	33000-01	79.72397	0.54839					
Hornblende	33000-03	79.64110	0.41550					
	33000-05	79.92520	0.21257					
	33000-06	79.79686	0.26976					
	33000-07	79.99423	0.21664					
	33000-08	79.85893	0.32670					
	33000-11	79.57674	0.21405					
	33000-14	79.90703	0.26277					
	33000-15	80.26145	0.20002					
	33000-18	79.57250	0.46829					
	33000-20	80.21144	0.40518					
FCs	33001			0.58912	0.00051			
Summary		79.90788	0.08231	0.58912	0.00051	135.63893	0.18206	0.134

Notes. Samples are described in Appendix A2. F values refer to $^{40}Ar^*/^{39}Ar_K$; R values as defined in text. Summary values are weighted (by inverse variance) means. FCs data are from grains in the same irradiation disk pit as the sample in all but the case of PR94-7 ([a]), where FCs from three pits bracketing the sample were averaged and the mean and standard deviation are used. For sample SH-10, the Previous Data ([b]) are from Renne et al. (1995).

To be included in our analysis, $^{206}Pb/^{238}U$ ages must be concordant with $^{207}Pb/^{235}U$ ages at the 95%-confidence level using the concordia-age algorithms of Ludwig (1998), specifically including decay constant uncertainties. Normalization of $^{40}Ar/^{39}Ar$ ages in this study is restricted to the ^{238}U–^{206}Pb decay system, as recommended by Steiger and Jäger (1977), eliminating the effects of ^{235}U decay-constant uncertainties (Mattinson, 1987; Ludwig, 1998, 2000) and/or open-system behavior on the uncertainties of $^{207}Pb/^{206}Pb$ and concordia-intercept ages. $^{206}Pb/^{238}U$ data from multiple single-zircon analyses must be statistically coherent at the 95%-confidence level to avoid (as much as possible) averaging complexities arising from Pb-loss and/or subtle inheritance of pre-eruptive crystals. Pretreatment of most zircon samples with the anneal-leach technique pioneered by Mattinson (2005) produced results consistent with closed isotopic systems, eliminating a need for arbitrary selection from complex data sets.

To be used for our analysis, $^{40}Ar/^{39}Ar$ data must exhibit excellent reproducibility and demonstrable freedom from the effects of secondary alteration or ^{39}Ar recoil. Strict attention to determining the neutron fluence, and accounting for possible fluence gradients during sample irradiation, is required. Non-atmospheric initial ^{40}Ar must be absent or precisely characterized by isochron analysis. Data from pyroclastic rocks must be obtained from single crystals to avoid xenocrystic contamination. Age spectra obtained by incremental heating must define a plateau (*sensu* Fleck et al., 1977) containing >90% of the ^{39}Ar released and lacking statistically significant slope.

U–Pb and $^{40}Ar/^{39}Ar$ analyses were performed at the Berkeley Geochronology Center using facilities and procedures described previously (Min et al., 2000; Mundil et al., 2001, 2004) except as noted, with results summarized in Electronic Annexes EA-1 and EA-2 respectively. Descriptions of samples lacking previously published data are given in the Appendix. Some additional data from the literature which meet our criteria are also included. The volcanic rocks span an age interval between ca. 17 and 2068 Ma. $^{206}Pb/^{238}U$ ages include uncertainty in the ^{238}U decay constant, tracer calibration, and correction for initial ^{230}Th. $^{40}Ar/^{39}Ar$ results are represented by R-values as defined in Eq. (2) relative to Fish Canyon sanidine. The results used to compute weighted (by inverse variance) mean R-values from $^{40}Ar/^{39}Ar$ data presented in Electronic Annex EA-2 are summarized in Table 3. $^{40}Ar/^{39}Ar$ ages corresponding to these R-values, using the decay constants of Steiger and Jäger (1977) and the standard calibration of Renne et al. (1998), hereinafter referred to as "conventional" $^{40}Ar/^{39}Ar$ ages, are compared with the $^{206}Pb/^{238}U$ ages in Fig. 1.

The data pairs of $^{206}Pb/^{238}U$ and conventional $^{40}Ar/^{39}Ar$ ages presented here exhibit a systematic bias such that the $^{206}Pb/^{238}U$ ages are older than the $^{40}Ar/^{39}Ar$ ages. The bias ranges from >1.5% for young rocks to ca. 0.5% for rocks as old as 2 Ga. A bias of this magnitude resulting from miscalibrated artificial tracers used in isotope dilution U/Pb analyses is not expected as recent cross-calibrations of the U/Pb ages presented here are comparable at the 0.15% level with ages from other state-of-the-art laboratories (Black et al., 2004). A potential variation of λ_ε due to changing physical and chemical environments has been shown to be even less significant (Bukowinski, 1979; Norman et al., 2001). Instead, the magnitude and observed pattern of data pairs (bias decreasing as a function of age) can most easily be explained by two independent contributing factors: pre-eruptive residence time and mis-estimation of the ^{40}K decay constants.

Pre-eruptive magma residence times for zircons, which have been observed to be as large as ca. 300 ka, can have a significant impact on relatively young rocks (such as sample IP of this study), but their importance should diminish linearly with age. In other words, if residence time was the sole reason for the bias in all samples depicted in Fig. 1(a), the observed bias of 400 ka to 13 Ma could only be explained by a correlation between age and residence time. This is implausible not only because there is no physical mechanism to produce such a correlation, but also because

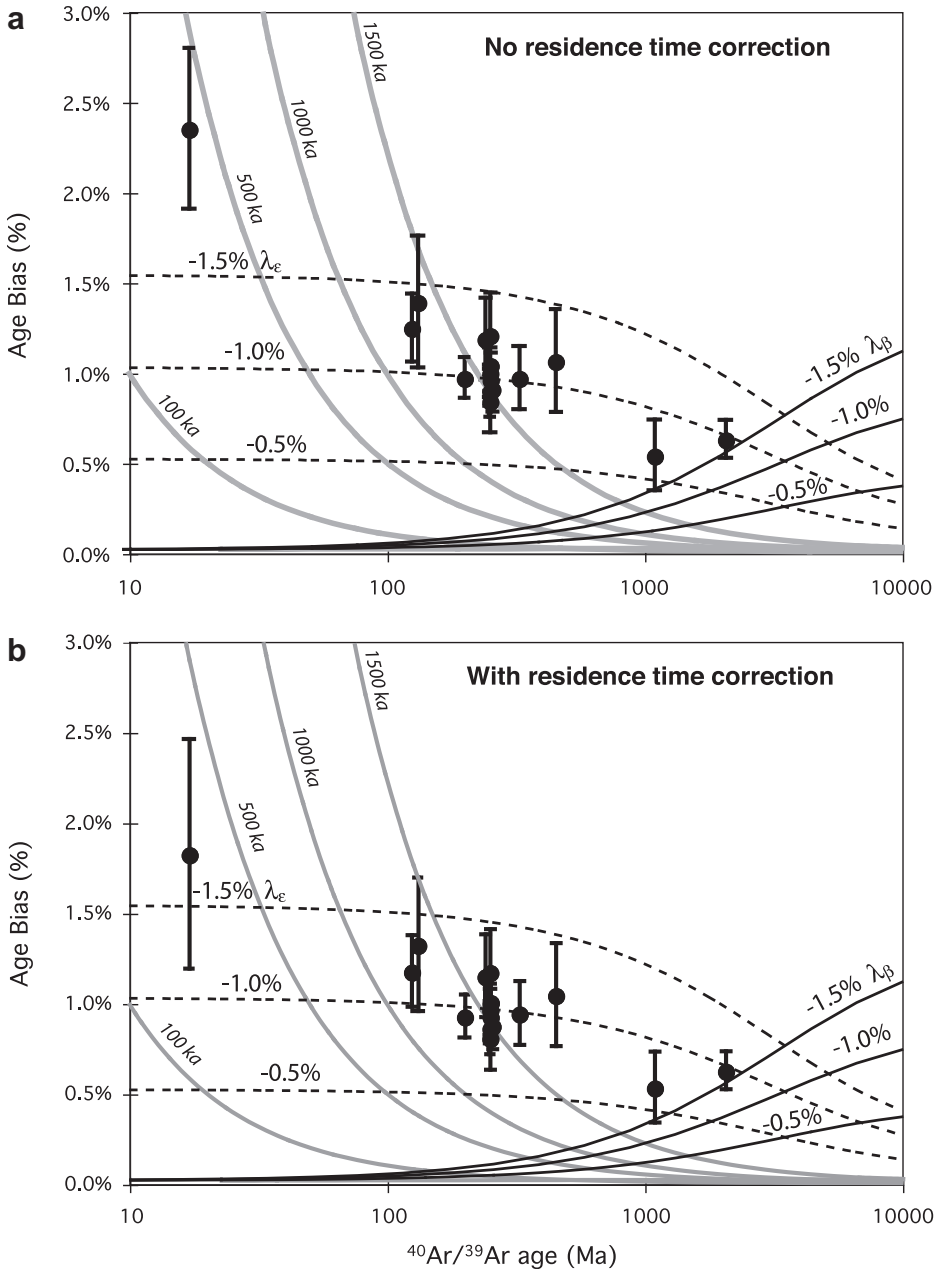

Fig. 1. Bias between $^{238}U/^{206}Pb$ zircon ages and "conventional" calibration of the $^{40}Ar/^{39}Ar$ system for data pairs listed in Table 2. Upper panel (a) shows $^{238}U/^{206}Pb$ zircon ages uncorrected for residence time effects. Lower panel (b) shows the effect of correcting for residence time of 90 ± 77 ka (see text for discussion). For comparison are shown curves depicting the effects of: (i) 100–1500 ka zircon residence times (solid gray); (ii) decreasing the electron capture decay constant for ^{40}K by 0.5%, 1.0%, and 1.5% (dashed black); and (iii) similarly decreasing the beta decay constant of ^{40}K (solid black).

zircon residence times greater than 1 Ma would be required for all of the >100 Ma samples – much longer than any case documented to date. Inherited zircons or antecrysts (e.g., Bacon and Lowenstern, 2005) exhibiting such pre-eruptive age are not uncommon, but in cases considered here are ruled out by the statistical coherence of the individual zircon $^{206}Pb/^{238}U$ ages.

In Fig. 1(b) we recalculated the $^{206}Pb/^{238}U$ ages assuming that they all include a pre-eruptive residence time of 90 ± 77 ka derived from the compilation of Simon et al. (2008). Although further studies are desirable to clarify the scope of residence time manifest in zircon U–Pb ages, the correction we use is an objective measure given the current state of knowledge. The recalculation consists of simply subtracting 90 ± 77 ka from each $^{206}Pb/^{238}U$ age and propagating the additional uncertainty such that if the uncorrected $^{206}Pb/^{238}U$ age uncertainty is σ_τ, the uncertainty on the corrected $^{206}Pb/^{238}U$ age σ'_τ becomes $\sqrt{\sigma_\tau^2 + (77\ \text{ka})^2}$. This adjustment slightly reduces $^{206}Pb/^{238}U$ ages, and slightly

increases their uncertainties. As discussed later, we adopt this correction to the $^{206}Pb/^{238}U$ ages and their uncertainties in the regression analysis. After accounting for residence time bias in this way, there is still a tendency for the bias to decrease as a function of age although all the individual results are indistinguishable at 95% confidence from a 1% bias. This tendency is easily explained in sense and magnitude by miscalibration of λ_ε, whose relative uncertainty from disintegration counting is the largest among the three variables considered here.

Whereas the ca. −1% bias implying miscalibration of λ_ε is well constrained for Phanerozoic samples, a decrease of the bias to ca. −0.5% (possibly even lower) for older ages (as displayed by the data pairs from F-239 and EGB-032 at 1.09 and 2.06 Ga, respectively), is less confidently attributed to this source. Rather, miscalibration of λ_β in the opposite sense is suggested, consistent with the previously discussed LSC data which indicate a ~0.22% larger value ($5.555 \times 10^{-10}\ a^{-1}$) of λ_{tot} than that ($5.543 \times 10^{-10}\ a^{-1}$) recommended by Steiger and Jäger (1977). This hypothesis is addressed more thoroughly by the regression analysis described later.

Several data sets are excluded from our analysis that might seem appropriate to include. Specifically, U–Pb zircon data from the Fish Canyon Tuff (FCT) itself could be highly relevant in principle to our analysis. Unfortunately, such data from the FCT (Schmitz and Bowring, 2001; Bachman et al., 2007) and two additional eruptive units from the same magma system (Bachman et al., 2007) reveal excess dispersion (i.e., having MSWD values ranging from 6 to 18) in $^{206}Pb/^{238}U$, and thereby fail the equivalence (*sensu* Ludwig, 1998) criterion employed to exclude data affected by Pb-loss and/or subtle inheritance. We note here that although Schmitz and Bowring (2001) reported a seemingly reasonable MSWD of 0.97 for their FCT zircon data, Bachman et al. (2007) showed that this was an artifact of a calculation error, and that the true MSWD is ~10. The excess scatter manifest in U–Pb data for all three units from this magma system probably arises – at least in part – from pre-eruptive residence time, but the observed non-analytical scatter in the individual dates precludes any confidence that Pb-loss has been completely mitigated, or that the effects of subtle inheritance and/or antecrysts are absent. A similar caveat applies to $^{206}Pb/^{238}U$ – $^{40}Ar/^{39}Ar$ data pairs reported for tuffs in the Green River Formation (Smith et al., 2010), wherein excess scatter in $^{206}Pb/^{238}U$ ages violates our equivalence criterion and subjective data culling is required to interpret an age. Therefore these data, despite their excellent analytical quality, are excluded from our analysis although we note that excess scatter of similar magnitude could be present (though unrecognizable) in older samples including those used in this study.

2.6. Other (τ_i, R_i) pairs

In addition to samples with $^{40}Ar/^{39}Ar$ data whose age is independently constrained by $^{206}Pb/^{238}U$ dates, there are several additional data pairs possible in which the independent constraints are provided by other means. Renne and Min (1998) proposed such an approach using $^{40}Ar/^{39}Ar$ data for sanidine from the historically dated Vesuvius eruption of 79 CE (Common Era). Although Renne and Min (1998) used a different standard (ACs) as a neutron fluence monitor, their results can be related to FCs using the definitions and data given by Renne et al. (1998), such that $R_{FCs}^{AD79} \equiv R_{ACs}^{AD79} \cdot R_{FCs}^{ACs} = (6.789 \pm 0.055) \times 10^{-5}$, as used by Kwon et al. (2002). The relevant age for comparison (in CE 1998, when the measurements were made or normalized to) is 1.919 ka, and we include this data pair in our analysis despite the relative imprecision (±0.8%) of the *R*-value.

Another set of (τ_i, R_i) pairs that might be included are those from Kuiper et al. (2008) that consist of $^{40}Ar/^{39}Ar$ data relative to FCs for Miocene tuffs in the Melilla Basin of Morocco whose absolute ages can be inferred from astronomical tuning, that is, correlating stratigraphic climate proxy records with calculated orbitally modulated terrestrial insolation time series. These data would complement the $^{206}Pb/^{238}U$-constrained data pairs well because they are relatively young, but not affected by pre-eruptive residence time. However, because ages derived from astronomical tuning are based on one-to-one correlation of stratigraphic units with insolation cycles rather than on analyses with well-defined uncertainty distributions, it is difficult to estimate their uncertainty in a way that is compatible with measurement uncertainties on our other input data. Thus, we exclude these results from the present analysis and instead, as discussed later, use them as a basis for independent comparison.

3. DATA ANALYSIS

We seek to find values for the parameters λ_ε, λ_β, and κ_{FCs} that best fit: (i) the relations described by Eq. (3) and the (τ_i, R_i) pairs described in the Introduction (Section 1) and Section 2.5, as well as (ii) the independent measurements of these parameters described in Sections 2.1–2.4. We adapt the nonlinear regression model of Kwon et al. (2002) for this purpose. First, we rewrite Eq. (3) to predict a value for the true age of a sample τ_i^* given estimates of R_i^*, λ_ε^*, λ_β^*, and κ_{FCs}^*. The superscripted star denotes estimates for the various quantities that are generated by the solution method, as opposed to the independently measured values of these quantities that comprise the data set we seek to fit. This yields:

$$\tau_i^* = \left(\frac{1}{\lambda_\varepsilon^* + \lambda_\beta^*}\right) \ln\left[\left(\frac{\lambda_\varepsilon^* + \lambda_\beta^*}{\lambda_\varepsilon^*}\right)\kappa_{FCs}^* R_i^* + 1\right] \quad (4)$$

Following Kwon et al. (2002), the best estimates of λ_ε^*, λ_β^*, and κ_{FCs}^* are found by minimizing the sum of squares *S*:

$$S(X) = \sum_{i=1}^{n}\left[\frac{1}{2}\left(\frac{\tau_i^* - \tau_i}{\sigma_{\tau,i}}\right)^2 + \frac{1}{2}\left(\frac{R_i^* - R_i}{\sigma_{R,i}}\right)^2\right] \quad (5)$$

over $X = (\lambda_\varepsilon^*, \lambda_\beta^*, \kappa^*, R_1^*, R_2^*, \ldots, R_n^*)$. Here $\sigma_{\tau,i}$ and $\sigma_{R,i}$ are measurement uncertainties in τ_i and R_i, respectively (Table 2). Note that this procedure also yields optimized estimates of the *R* values of all the samples in our data set, though these are nuisance parameters for the present purpose. Minimizing $S(X)$ yields parameter values that best

fit the (τ_i, R_i) pairs, but our overall goal in this work is to incorporate all pertinent information, including both the (τ_i, R_i) pairs and the independent measurements of κ_{FCs} and the decay constants, into our estimates of these quantities. Thus, we find values of λ_ε^*, λ_β^*, and κ_{FCs}^* that best fit both the (τ_i, R_i) pairs and the independent measurements λ_ε, λ_β, λ_{tot}, and κ_{FCs} by minimizing

$$S_1(X) = S(X) + \left(\frac{\lambda_\varepsilon^* - \lambda_\varepsilon}{\sigma_{\lambda\varepsilon}}\right)^2 + \left(\frac{\lambda_\beta^* - \lambda_\beta}{\sigma_{\lambda\beta}}\right)^2 + \left(\frac{\kappa_{FCs}^* - \kappa_{FCs}}{\sigma_{K_{FCs}}}\right)^2 + \left(\frac{\lambda_{tot}^* - \lambda_{tot}}{\sigma_{\lambda_{tot}}}\right)^2 \quad (6)$$

over $X = (\lambda_\varepsilon^*, \lambda_\beta^*, \kappa_{FCs}^*, R_1^*, R_2^*, \ldots, R_n^*)$. Here λ_ε, λ_β, λ_{tot}, and κ_{FCs} (lacking superscripted asterisks) are the independently measured values of these quantities described above in Section 2, and $\sigma_{\lambda\varepsilon}$, $\sigma_{\lambda\beta}$, $\sigma_{\lambda tot}$, and $\sigma_{K_{FCs}}$ are their respective measurement uncertainties (Table 1). An important aspect of this approach is that the independent estimate of each of these parameters is given the same weight as any one of the (τ_i, R_i) pairs.

As previously discussed in Section 2, we adjusted all values of τ_i in Table 2 that are derived from $^{206}Pb/^{238}U$ measurements by subtracting a pre-eruptive residence time of 90 ± 77 ka. Although this correction acts to slightly improve the optimal value of S_1, we applied it not for this reason but because of the first-principles observation that pre-eruptive residence time is common and, therefore, that a correction is required. We then actually carried out the minimization using the MATLAB implementation of the Nelder–Mead simplex search method (Lagarias et al., 1998), and estimated uncertainties in the best-fitting parameter values by a 4000-trial Monte Carlo simulation. With one exception, all measurement uncertainties in the input parameters were assumed to be Gaussian and independent. The exception is that the uncertainties in the $^{206}Pb/^{238}U$ ages are not independent, because of their common dependence on the ^{238}U decay constant. We incorporated this effect into the Monte Carlo simulation by: (i) transforming $^{206}Pb/^{238}U$ ages and their uncertainties to ratios of radiogenic ^{206}Pb to ^{238}U ($^{206}Pb^*/^{238}U$) and corresponding uncertainties using the Jaffey et al. (1971) value and uncertainty for $\lambda(^{238}U)$; (ii) for each trial, randomly generating values of $^{206}Pb^*/^{238}U$ for all samples as well as a single common value of $\lambda(^{238}U)$; and (iii) using these to compute trial values of τ_i. This procedure produces a random sample of τ_i values that display the covariance resulting from their common dependence on the ^{238}U decay constant.

4. OPTIMIZATION RESULTS

Tables 4a–c show the values of λ_ε^*, λ_β^*, κ_{FCs}^*, and $R_1^*, R_2^*, \ldots, R_n^*$ that minimize S_1, as well as the implied values of τ_i^*. These best-fit values yield $S_1 = 8.8$. Table 4, Figs. 2 and 3 show the results of the Monte Carlo error analysis. Fig. 4 shows the distribution of the normalized residuals with respect to the input values of τ_i, R_i, λ_ε, λ_β and κ_{FCs}; the distribution is indistinguishable from normal. We did not observe any significant relationship between the

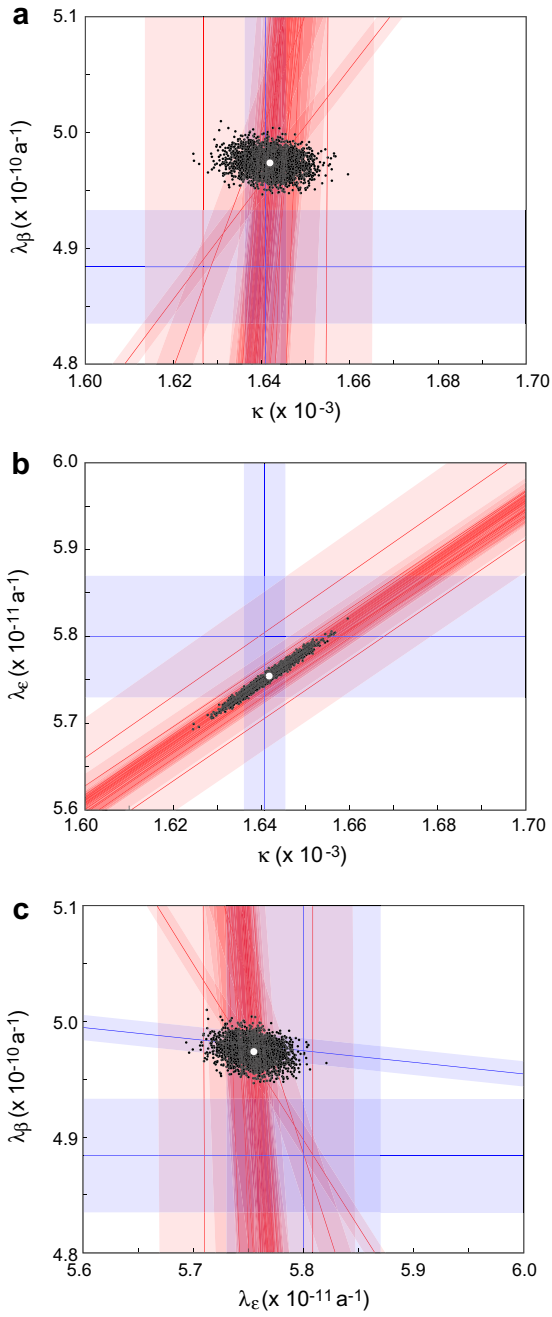

Fig. 2. Optimal values of the parameters κ_{FCs}, λ_ε, and λ_β, and results of the Monte Carlo error analysis compared with constraints used as input to the regression analysis. Each panel has two of these parameters as its axes, and the constraints are evaluated at the optimal value, given in Table 4a, of the third parameter. For example, in the panel with axes κ_{FCs} and λ_ε, the constraints are computed with λ_β fixed at 4.9737×10^{-10} a^{-1}. The open circles show the optimal values of the parameters. The black dots show projections normal to the plane of each panel of the results of the Monte Carlo error analysis. The blue lines and blue shaded regions represent planes and corresponding 68% confidence regions defined by the independent parameter measurements in Table 1. The red lines and red shaded regions represent surfaces and corresponding 68% confidence regions defined by Eq. (3) evaluated for each of the (τ_i, R_i) pairs in Table 3.

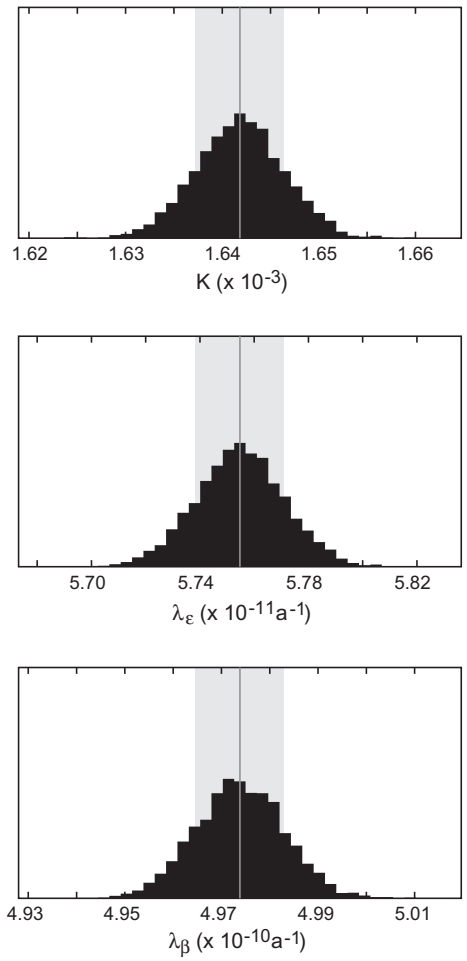

Fig. 3. Marginalized probability distributions for the parameters κ_{FCs}, λ_ε, and λ_β derived from the Monte Carlo error analysis. The dark vertical line shows the optimal value of each parameter, and the grey band shows the standard deviation of each parameter computed from the Monte Carlo results.

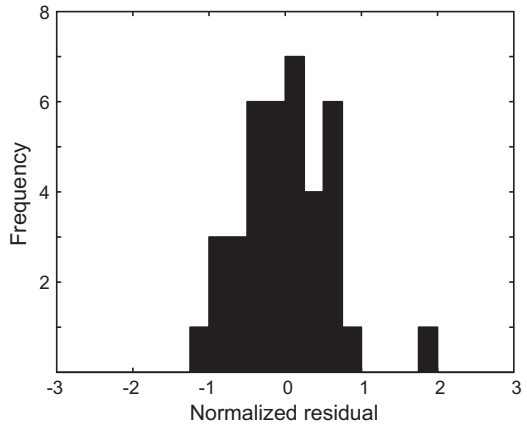

Fig. 4. Frequency distribution of normalized residuals for the best-fitting values of λ_ε^*, λ_β^*, κ_{FCs}^*, R_1^*, $R_2^*, \ldots, R_n^*$, and the implied values of τ_i^*, and the corresponding measurements and their uncertainties.

residuals with respect to R_i and τ_i and the values of R_i and τ_i themselves. One can evaluate the quality of the fit by computing, for example, the reduced chi-squared (χ_R^2) statistic of the best-fitting values of λ_ε^*, λ_β^*, κ_{FCs}^*, R_1^*, $R_2^*, \ldots, R_n^*$, and the implied values of τ_i^* with respect to the corresponding measurements and their uncertainties: here $\chi_R^2 = 0.75$ for 18 degrees of freedom. This is close to the expected value of 1, with a probability-of-fit of 0.76, indicating that the scatter of the measurements with respect to the best-fitting parameter values is consistent with measurement uncertainties. We conclude that: (i) these best-fitting values for λ_ε^*, λ_β^*, and κ_{FCs}^* successfully reconcile all paired $^{40}Ar/^{39}Ar$ and $^{206}Pb/^{238}U$ ages as well as the independent measurements of the parameters and (ii) all relevant measurements incorporated in the regression analysis are consistent at the level of their stated uncertainties.

5. APPLICATION OF THE RESULTS

Comparison of Tables 1 and 4a shows that our estimates of λ_ε^* and λ_β^* are significantly more precise than previously determined values, while the precision of our estimate of κ_{FCs}^* remains essentially unchanged.

5.1. Age uncertainties

We now draw attention to two additional aspects of the results that are critically important in using these parameter estimates to compute $^{40}Ar/^{39}Ar$ ages and their uncertainties. First, it is important to make clear that because we are estimating all three parameters needed for computing $^{40}Ar/^{39}Ar$ ages simultaneously, these parameter estimates are not independent. In fact, as shown by the Monte Carlo results in Fig. 2, the uncertainties on these parameters are strongly correlated. This contrasts with the previous measurements shown in Table 1, which were determined in separate experiments with independent uncertainties. One must take the covariance into account in error propagation when calculating $^{40}Ar/^{39}Ar$ ages using our estimates of λ_ε^*, λ_β^*, and κ_{FCs}^*. Using linear error propagation, the uncertainty in an $^{40}Ar/^{39}Ar$ age calculated using Eq. (4) is:

$$\sigma_t^2 = \left(\frac{\partial t}{\partial \lambda_\varepsilon}\sigma_{\lambda_\varepsilon}\right)^2 + \left(\frac{\partial t}{\partial \lambda_\beta}\sigma_{\lambda_\beta}\right)^2 + \left(\frac{\partial t}{\partial \kappa_{FCs}}\sigma_{\kappa_{FCs}}\right)^2 + \left(\frac{\partial t}{\partial R}\sigma_R\right)^2 + 2\frac{\partial t}{\partial \lambda_\varepsilon}\frac{\partial t}{\partial \kappa_{FCs}}\mathrm{cov}(\lambda_\varepsilon, \kappa_{FCs}) + 2\frac{\partial t}{\partial \lambda_\beta} \times \frac{\partial t}{\partial \kappa_{FCs}}\mathrm{cov}(\lambda_\beta, \kappa_{FCs}) + \frac{\partial t}{\partial \lambda_\varepsilon}\frac{\partial t}{\partial \lambda_\beta}\mathrm{cov}(\lambda_\varepsilon, \lambda_\beta) \quad (7)$$

Table 4a
Optimization results: optimal values of parameters needed to compute a $^{40}Ar/^{39}Ar$ age (K, $\lambda_\varepsilon\lambda_\beta$) as well as the value of λ_{tot} implied by these results. The uncertainties are derived from the Monte Carlo error analysis.

Variable	Value	$\pm\sigma$	$\pm\%$
κ_{FCs}	1.6418×10^{-3}	0.0045×10^{-3}	0.27
λ_ε	0.5755×10^{-10} a^{-1}	0.0016×10^{-10} a^{-1}	0.28
λ_β	4.9737×10^{-10} a^{-1}	0.0093×10^{-10} a^{-1}	0.19
λ_{tot}	5.5492×10^{-10} a^{-1}	0.0093×10^{-10} a^{-1}	0.17

Table 4b
Optimization results: covariances and error correlations between parameters needed to compute a $^{40}Ar/^{39}Ar$ age (K, $\lambda_\varepsilon\lambda_\beta$), derived from the Monte Carlo error analysis.

Variables (x,y)	Covariance cov(x,y)	Error correl. $\rho_{x,y}$
$(\kappa_{FCs},\lambda_\varepsilon)$	7.1889×10^{-19}	0.9985
$(\kappa_{FCs},\lambda_\beta)$	-7.1390×10^{-19}	−0.1706
$(\lambda_\varepsilon,\lambda_\beta)$	-3.4497×10^{-26}	−0.2318

This includes covariance terms for λ_ε, λ_β, and κ_{FCs}. A measurement of R is independent of these parameters, so the covariance terms involving R are zero and are omitted.Solutions of the partial derivatives in Eq. (7) are given in Appendix A.2 and the covariances are as given in Table 4b along with the corresponding error correlations defined by $\rho_{x,y} = \text{cov}(x, y)/(\sigma_x\sigma_y)$. The covariance terms in this expression have a significant effect on the uncertainty of an $^{40}Ar/^{39}Ar$ age computed from the data in Table 4a. For example, a hypothetical sample with $R = 50 \pm 0.25$ (a 0.5% uncertainty) has an age of 1050.7 Ma. The uncertainty in this age calculated (incorrectly) ignoring the covariance terms in Eq. (7) would be ±5.1 Ma; the correct uncertainty that takes account of the covariance terms is ±4.0 Ma. A graphical explanation of this effect is as follows. Finding the values of λ^*_ε, λ^*_β, and κ^*_{FCs} that minimize Eq. (5) is in effect finding values of these parameters that best reconcile $^{40}Ar/^{39}Ar$ and U/Pb ages. Graphically, this can be thought of as seeking points that are near the mutual intersection of the surfaces defined by Eq. (3) applied to the various (τ_i, R_i) pairs. As is evident from Fig. 2, these intersections are nearly colinear in the region of interest. Thus, parameter values can be relatively widely scattered with respect to any one of the individual parameters, but if they remain close to this region of intersection they will still precisely reconcile $^{40}Ar/^{39}Ar$ and U/Pb ages.

A second important issue for applying our results is that the uncertainties and covariances reported in Tables 4a and b are derived via Monte Carlo simulation, so are not arbitrarily precise. In addition, Eq. (7) above is an approximation derived by linearizing Eq. (4). For these reasons, Eq. (7) with the uncertainties and covariances in Tables 4a and b may yield age uncertainties that are inaccurate when uncertainties in R are less than approximately 1 per mil. Thus, one should use a Monte Carlo method rather than linear error propagation to compute age uncertainties when the uncertainties in R are small. We supply in EA-3 an Excel spreadsheet containing (i) 4000 (λ_ε, λ_β, and κ_{FCs}) triplets, that are derived from our Monte Carlo uncertainty analysis for these parameters and display the variances and covariances shown in Tables 4a and b, and (ii) a spreadsheet program for generating a normal distribution of R-values given an arbitrary input mean and standard deviation. This spreadsheet can be used straightforwardly for a Monte Carlo analysis of uncertainty in age calculations. Note that for computing ages themselves, the exact solution presented by Eq. (4) should be used; the age returned by the Monte Carlo approach will always be an approximation.

Relative age errors estimated by Eq. (7) are shown in Fig. 5 for values of R with relative precision between 0% and 1.0%. A noteworthy consequence of our results, illustrated in Fig. 5, is that the relative uncertainty of $^{40}Ar/^{39}Ar$

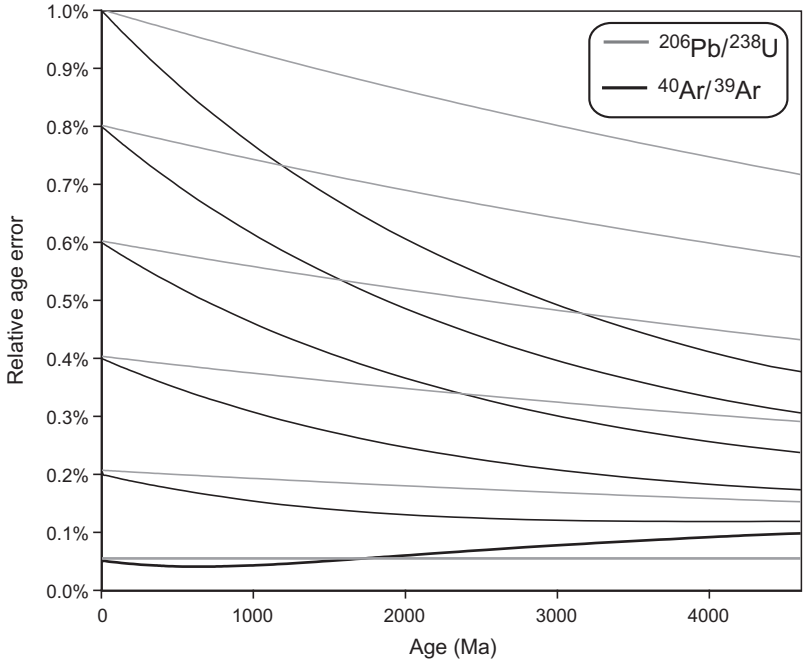

Fig. 5. Summary of the accuracy of $^{40}Ar/^{39}Ar$ ages calculated with the results of this work, compared with the $^{238}U/^{206}Pb$ system. Relative age errors are shown for different values of relative isotope measurement precision (σ_R/R) whose values correspond to the intercept on the ordinate (relative age error) axis; lowest (darker) curves correspond to infinitely precise R-values (zero uncertainty). For the $^{40}Ar/^{39}Ar$ system, R is as defined by Eq. (2) as the $^{40}Ar^*/^{39}Ar_K$ of a sample relative to that of the FCs standard. For the U/Pb system, R is defined as $^{206}Pb^*/^{238}U$.

ages is dramatically improved with increasing age (R-value) for relative σ_R greater than about 0.2%. While contraction in relative age error with increasing age is a consequence of the logarithmic relation between age and R, and is true for all radioisotopic age equations, the relationship shown in Fig. 5 is especially noteworthy in comparison with the $^{206}Pb/^{238}U$ system. Here, the R-value for $^{206}Pb/^{238}U$ is taken to be the $^{206}Pb^*/^{238}U$ ratio, and its uncertainty includes contributions from blank and mass fractionation corrections, spike calibration, etc. For $^{40}Ar/^{39}Ar$ ages, the R-values in Fig. 5 are as defined by Eq. (2) and also include corrections for blank and mass fractionation as well as decay and nucleogenic interferences. Thus the R-values and their uncertainties used for comparison of the two systems are not strictly equivalent, but they are comparable measures of the relevant mass spectrometric data and their accuracy.

An obvious implication of Fig. 5 is that with comparable measurement precision, the $^{40}Ar/^{39}Ar$ system can, with existing techniques, produce ages with accuracy comparable to or even exceeding the $^{206}Pb/^{238}U$ system. In effect this potential can now be realized because we have calibrated the $^{40}Ar/^{39}Ar$ system to both the ^{238}U and ^{40}K decay constants. This does not suggest that the $^{40}Ar/^{39}Ar$ method is necessarily preferable to the U/Pb method in cases where both are applicable, such as cases in which daughter-element mobility in the $^{40}Ar/^{39}Ar$ system is an issue, but it places the $^{40}Ar/^{39}Ar$ method on firm footing to validate even exceptionally precise U/Pb ages in cases where both are expected to record simultaneous closure to daughter nuclide mobility. Some examples follow.

5.2. Comparison with astronomical calibration

The previously-mentioned recent astronomical calibration of the age of the FCs standard (Kuiper et al., 2008) provided a significant breakthrough in reducing systematic errors and reconciling $^{40}Ar/^{39}Ar$ ages with ages determined by U/Pb and astronomical tuning. Application of the results of Kuiper et al. (2008) is based on Eq. (1) and the relationship between an unknown and the astronomically-dated horizon given by $R^{un}_{Ast} \equiv R^{un}_{FCs} \cdot R^{FCs}_{Ast} = R^{unk}_{FCs} \cdot (4.3644 \pm 0.0009)$. In this case the independent "true" age τ (6.500 ± 0.005 Ma) is determined independently by astronomical tuning as discussed in Section 2.6.

In comparing our results to the calibration of Kuiper et al. (2008), which was focused on the age of FCs, we first address the question of how $^{40}Ar/^{39}Ar$ ages based on this result compare to ages and age uncertainties computed using our calibration. We note that Kuiper et al. (2008) did not explicitly recommend a value for λ_{tot}, but their derivation of an age for FCs used the sum of the partial decay constants listed in Table 1, $(5.463 \pm 0.107) \times 10^{-10}$ a^{-1}, as described above. The λ_{tot} dependence of Eq. (1) introduces large propagated age errors for astronomically calibrated ages very different from τ_{Ast}. These age errors are significantly larger than those computed using our new calibration as shown in Fig. 6.

Ages computed from the astronomical calibration as described above are compared with those based on our new calibration in Fig. 7. The values of λ_ε, λ_β, and κ_{FCs} determined herein yield older ages (by 0.38%) at zero age, and younger ages (by 0.86%) at 4560 Ma than those computed using the astronomical calibration. However, due mainly to the large uncertainties in the latter, the differences between ages based on the two calibrations are not significant at 95% confidence except for ages <100 Ma with precisely determined R-values ($\sigma_R/R < 0.1\%$).

Second, we ask whether the (τ, R) pair itself determined by the combination of astronomical tuning and $^{40}Ar/^{39}Ar$ analysis relative to FCs is consistent with our independent calibration. To do this, we used the relationship $R^{Ast}_{FCs} = (R^{FCs}_{Ast})^{-1} = 0.229127 \pm 0.000047$ to compute an age based our values of λ_ε, λ_β, and κ_{FCs}. The resulting age is

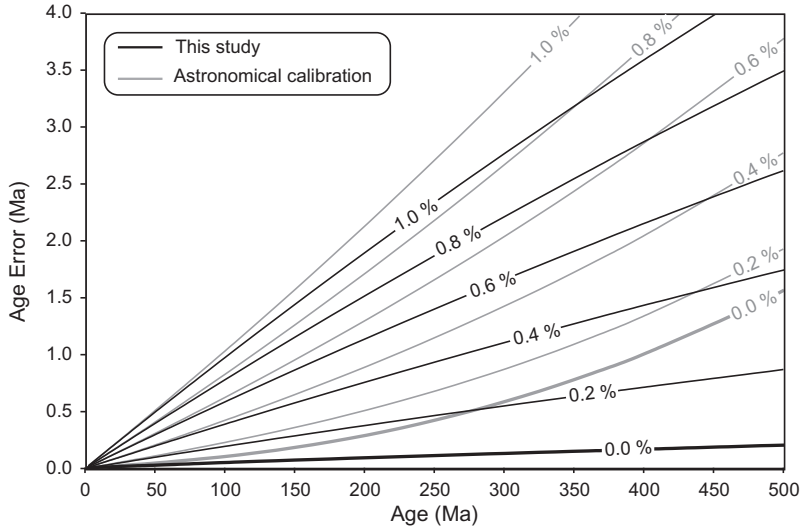

Fig. 6. Age uncertainties as a function of age for calibration of the $^{40}Ar/^{39}Ar$ system presented herein versus that of Kuiper et al. (2008) based on astronomical tuning for the age of FCs and the ^{40}K decay constant of Min et al. (2000). Contours show results for various relative uncertainties in R.

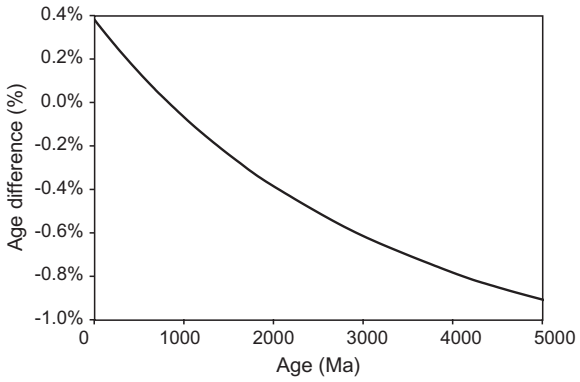

Fig. 7. Difference between ages determined from data presented herein versus those based on the astronomical age of Kuiper et al. (2008) for FCs.

6.525 ± 0.005 Ma (error computed using Monte Carlo simulation), which can be compared with the astronomically tuned age of 6.500 ± 0.005 Ma reported by Kuiper et al. (2008). The difference between these ages, 25 ± 7 ka, is significant at 95% confidence. Though this age difference is indistinguishable from the duration of a single orbital precession cycle, this may be serendipitous as the astronomical tuning of Kuiper et al. (2008) is based on orbital eccentricity and obliquity as well as precession, whose combined effect on insolation is the tuning basis. The cause of the discrepancy should be addressed by future work.

5.3. Implications for selected $^{40}Ar/^{39}Ar$ ages

Several implications of the revised constants proposed here bear discussion. We focus on the consequences for $^{40}Ar/^{39}Ar$ standards and a few other selected samples shown in Table 5. Although our results in general greatly improve consistency between ages determined by the $^{40}Ar/^{39}Ar$ system and those determined by other techniques, in some cases the new calibrations reveal inconsistencies that warrant further consideration. The recalculated age of FCs – 28.305 ± 0.036 Ma, including systematic errors – is an iconic manifestation of the results. For the age uncertainty calculation in this case we assumed a relative uncertainty of 0.11% for the *R*-value, corresponding to the average reproducibility of $^{40}Ar^*/^{39}Ar_K$ reported by Renne et al. (1998). This age is distinguishable from the astronomically-tuned age of 28.201 ± 0.023 Ma (Kuiper et al., 2008) at 95% confidence, and this discrepancy remains to be further investigated. Recalculated $^{40}Ar/^{39}Ar$ ages of several other standards that have been intercalibrated with FCs are shown in Table 5. Alder Creek sanidine (ACs), Taylor Creek sanidine (TCs), GA-1550 biotite, and Hb3gr hornblende all yield age accuracies better than or equal to 0.16% when systematic errors in λ_ε, λ_β, and κ_{FCs} are included. NL-25 hornblende has a larger uncertainty of 0.38% including systematic errors, largely due to the imprecision (0.72%) of the *R*-value relating it to FCs.

The recalculated $^{40}Ar/^{39}Ar$ age (1.206 ± 0.002 Ma including systematic errors) of the Alder Creek sanidine (ACs) standard may be compared with independent estimates for the age of the Cobb Mountain geomagnetic polarity subchron recorded by its host rhyolite. Unfortunately the various estimates for the age of this event are too dispersed to provide an authoritative independent validation (e.g., see discussion by Nomade et al., 2005 and references therein). However, we note that the most accurate age range (1.215–1.190 Ma) is likely that inferred by Channell et al. (2002) from high sedimentation rate cores in the Iceland Basin, where high resolution magnetostratigraphy and oxygen isotope stratigraphy permitted astronomical tuning with an estimated resolution of ±5 ka. Thus the recalculated $^{40}Ar/^{39}Ar$ age for ACs remains consistent with this rather broad independently estimated age range.

The recalculated $^{40}Ar/^{39}Ar$ age (99.77 ± 0.11 Ma including systematic errors) for GA-1550 biotite is significantly older than the 99.12 ± 0.07 Ma age inferred from $^{206}Pb/^{238}U$ data for 10 of 20 zircons analyzed from sample RSES01-98 by Schoene et al. (2006). These ages are clearly distinct at 95% confidence, and an older age for Ar closure in biotite than for Pb retention in zircon is unexpected for this rock unit, which is an intrusive monzonite. One of

Table 5
Recalculated $^{40}Ar/^{39}Ar$ ages of some standards and samples dating selected events in Earth history.

Standard or datum	R	$\pm\sigma$	$\pm\sigma$	Age (Ma)	$\pm\sigma$ (Ma)	$\pm\sigma$ (%)
BTs	0.02729	0.00013	0.48	0.7784	0.0037	0.48
ACs	0.04229	0.00006	0.14	1.2061	0.0019	0.16
FCs	1.0000	0.0011	0.11	28.305	0.036	0.13
TCs	1.0112	0.0010	0.10	28.619	0.034	0.12
KTB	2.3650	0.0015	0.06	66.236	0.060	0.09
GA-1550	3.5958	0.0031	0.09	99.769	0.108	0.11
PTB	9.4918	0.0038	0.04	252.27	0.18	0.07
Hb3gr	51.878	0.0592	0.11	1080.4	1.1	0.10
NL-25	211.42	1.52	0.72	2648.1	10.1	0.38

R-values are calculated using Eq. (2) and the following sources: BTs (Bishop tuff)- Sarna-Wojcicki et al. (2000); ACs – Nomade et al. (2005); TCs – Renne et al. (1998); KTB (Cretaceous/Tertiary boundary) – Swisher et al. (1993); GA –1550-Jourdan and Renne (2007); PTB (Permian/Triassic boundary) – Renne et al. (1995); Hb3gr – Jourdan and Renne (2007); NL-25 – Jourdan and Renne (2007). Age errors were calculated using Monte Carlo simulation (EA-3).

the twenty zircons analyzed by Schoene et al. (2006) yielded a $^{206}Pb/^{238}U$ age of 99.64 ± 0.03 Ma, indistinguishable from the $^{40}Ar/^{39}Ar$ age, raising the possibility that the younger cluster at 99.12 ± 0.07 Ma is biased by Pb-loss. This is speculative, however, and we cannot confidently explain the discrepancy.

The age of the Cretaceous/Tertiary boundary, as represented by $^{40}Ar/^{39}Ar$ data for sanidine from the IRZ tonstein dated by Swisher et al. (1993), is recalculated to 66.236 ± 0.060 Ma, including systematic errors. This age is slightly older than that of 65.957 ± 0.040 Ma (Kuiper et al., 2008) estimated from astronomical tuning, and the difference (279 ± 72 ka) is significant at the 95% confidence level. The disagreement in this case is not simply a further manifestation of previously noted inconsistency between our results and those of astronomical tuning in the Miocene Melilla basin, because the latter was derived from completely independent analysis of strata at Zumaia, Spain. While the difference is not distinguishable at 95% confidence from that of a 405 ka eccentricity cycle (the basis of the orbital tuning age), we also note that the original source of the $^{40}Ar/^{39}Ar$ age we recalculated (Swisher et al., 1993) did not document such details as neutron fluence gradients to justify an extremely precise (0.05% relative precision) *J*-value (a measure of the neutron fluence) ascribed to the sample. Hence it is unclear whether the $^{40}Ar/^{39}Ar$ age is as precise as stated. In any case, the discrepancy is worthy of further investigation.

The recalculated $^{40}Ar/^{39}Ar$ age (252.3 ± 0.2 Ma, including systematic errors) of the Permian–Triassic boundary involves one of the data pairs (Dt3) used as a constraint in this study. The $^{40}Ar/^{39}Ar$ age is indistinguishable from the $^{206}Pb/^{238}U$ zircon age of 252.4 ± 0.2 Ma reported by Mundil et al. (2004). Making an *ad hoc* residence time correction as discussed previously renders a $^{206}Pb/^{238}U$ age of 252.3 ± 0.2 Ma, which also coincides with the best-fit age – the age that is most consistent with all other data – given in Table 4c.

We recalculated the $^{40}Ar/^{39}Ar$ age of the Bishop Tuff from data originally reported by Sarna-Wojcicki et al. (2000) in order to compare the result with a $^{238}U/^{206}Pb$ zircon age reported by Crowley et al. (2007). These results fail our criteria for use in the regression employed here because of pronounced discordance between $^{238}U/^{206}Pb$ and $^{235}U/^{207}Pb$ ages, attributed by Crowley et al. (2007) to initial Pa/U disequilibrium. Seventeen of nineteen zircons reported by Crowley et al. (2007) yielded a $^{238}U/^{206}Pb$ age of 767.1 ± 0.5 ka, indistinguishable (at 95% confidence) from an inferred eruption age (770.4 ± 1.8 ka, recalculated from the $^{40}Ar/^{39}Ar$ data of Sarna-Wojcicki et al., 2000, using the standard calibration of Renne et al., 1998). Because of this inferred agreement between $^{238}U/^{206}Pb$ and $^{40}Ar/^{39}Ar$ ages, Crowley et al. (2007) concluded that "high-precision ID-TIMS geochronology can resolve magma chamber dynamics of <1 Ma silicic eruptions at the millennial scale". Moreover, because the majority of zircons were inferred to yield tightly clustered $^{238}U/^{206}Pb$ ages (after initial Th/U disequilibrium correction) coincident with eruption, Crowley et al. (2007) questioned the validity of ion probe U–Pb dates from Bishop Tuff zircons which have been inferred to document substantial residence times and protracted crystallization intervals (Simon and Reid, 2005). However, our recalculated $^{40}Ar/^{39}Ar$ age of the Bishop Tuff is 778 ± 4 ka (systematic errors included), resolvably older (by 11 ± 4 ka) than the age inferred from $^{238}U/^{206}Pb$ data by Crowley et al. (2007), suggesting that either the $^{40}Ar/^{39}Ar$ system in sanidine somehow records a pre-eruptive event, or that the $^{238}U/^{206}Pb$ age reported by Crowley et al. (2007) is biased for some reason (e.g., an inaccurate correction for initial Th/U disequilibrium).

Table 4c
Optimization results: optimal values of other parameters estimated in the regression analysis. As discussed in the text, the optimization scheme yields refined values for the measurements of R (denoted R_i^*); these, with the optimal values of the other parameters κ_{FCs}, λ_ε and λ_β, imply refined values for τ (denoted τ_i^*).

Sample	R_i^*	τ_i^* (Ma)
79CE	6.727×10^{-5}	1.919×10^{-3}
IP	0.6076	17.251
P1T-2	4.5531	125.43
PR94-7	4.8319	132.84
NMB	7.4616	201.21
MSG-09	9.0676	241.73
SH-10	9.4935	252.33
D3T	9.4919	252.29
SH-09	9.5087	252.71
PD97-2	9.5016	252.53
SH-27	9.5289	253.21
SH-16	9.5408	253.50
SH-08	9.6975	257.38
PaV	12.604	327.88
DK-LQ	18.114	454.37
F-239	52.796	1094.8
EGB-032	135.72	2066.9

A further implication of the calibration presented here is that the Brunhes/Matuyama geomagnetic polarity transition, which predates the eruption of the Bishop Tuff (Sarna-Wojcicki et al., 2000 and references therein), is older than 778 ± 4 ka. This constraint is consistent with the most precise available $^{40}Ar/^{39}Ar$ age for transitional polarity lavas from Maui ascribed to the transition (Coe et al., 2004), which is recalculated with the constants derived herein to 784 ± 2 ka, and is also consistent with some age estimates for the transition derived from orbital tuning, such as that (781 ka) summarized by Lourens et al. (2004). At face value, these results are marginally inconsistent with some other orbitally tuned chronologies for the Brunhes/Matuyama transition, such as those (~773 ka) reported by Channell et al. (2004). These apparent inconsistencies should be the focus of future investigations.

6. CONCLUSIONS

Here we have found values for the ^{40}K decay constants (λ_ε and λ_β), and the $^{40}Ar^*/^{40}K$ ratio (κ_{FCs}) of the FCs standard that best fit: (i) constraints from activity-based measurements of the ^{40}K decay constants, (ii) independent measurements of the age of the FCs standard, and (iii) paired U–Pb and $^{40}Ar/^{39}Ar$ ages on carefully selected samples. First, these esti-

mates of λ_ε and λ_β are significantly more accurate than obtainable from existing disintegration counting data alone. Second, uncertainties in these three parameter estimates are correlated, and the correlations must be accounted for in computing uncertainties of $^{40}Ar/^{39}Ar$ ages based on these results. Third, the fitting exercise shows that all these diverse constraints used as input data are mutually consistent at their stated uncertainties. Fourth, we have in effect calibrated the $^{40}Ar/^{39}Ar$ system with existing measurements of both the ^{40}K and ^{238}U decay constants. Thus, to the extent that uncertainties in these parameters represent the principal sources of systematic error in $^{40}Ar/^{39}Ar$ ages, our results imply approximately an order of magnitude improvement in the accuracy of the $^{40}Ar/^{39}Ar$ method relative to previous calibrations, over most of geologic time. Consequently, the $^{40}Ar/^{39}Ar$ method is now capable of accuracy comparable to that of the U/Pb system.

ACKNOWLEDGMENTS

This study was funded by the Ann and Gordon Getty Foundation augmented by NSF Grants EAR-9628065, EAR-9614324, EAR-9814378, and EAR-0451802. We thank M. Schmitz and S. Bowring, C. Swisher, and L. Black for providing samples EGB-032, PIT-2, and PaV, respectively; J. Bossi and N. Campal, and W. Sharp, for assistance in collecting samples PR94-7 and PD97-2, respectively. T. Becker, A. Deino and A. Jaouni are thanked for their various contributions to producing the data reported herein. Helpful comments on a manuscript draft by L. Morgan and J. Wijbrans are appreciated. Exceptionally constructive and thorough formal reviews by M. Cosca, F. Oberli, F. Albarede, B. Singer, and P. Reiners are gratefully acknowledged.

APPENDIX A

A.1. Sample notes

Most of the data used herein have previously been published, and the reader is referred to the original reference for information about the samples and data. Samples for which $^{40}Ar/^{39}Ar$ and/or $^{206}Pb/^{238}U$ data are being presented for the first time are discussed in further detail. In addition, notes about new data and other features of possible interest are included by sample.

79CE. $^{40}Ar/^{39}Ar$ (sanidine) data from this sample of pumice from the Plinian eruption of Vesuvius volcano near Pompei, Italy, were originally reported by Renne et al. (1997). New results from an additional sample were reported by Renne and Min (1998), whose combined results were corrected for the year between the two sets of analyses. The calendar year age is that in 1998 when the more recent isotopic data were measured.

IP. Sample IP is a rhyolite ignimbrite from the Gyulakeszi Rhyolite Tuff Formation exposed near Ipolytarnóc, Hungary, where it is associated with well-preserved Miocene ichnofossils. Both U/Pb and $^{40}Ar/^{39}Ar$ data were reported by Palfy et al. (2007) and those results are used herein.

PIT-2. (41° 35.6′ N, 120° 35.7′ E) Sample P1T-2 is a rhyolite tuff intercalated within fossil bearing Early Cretaceous terrestrial sediments of the Yixian Fm. from the Sihetun locality. Swisher et al. (1999) reported a weighted mean $^{40}Ar/^{39}Ar$ age of 124.60 ± 0.25 Ma for 35 single crystals of sanidine, and a plateau age of 124.6 ± 0.1 Ma for a step-heated multigrain aliquot. The sample is equivalent to, though not from the same collection as, sample YX07-4 from Chang et al. (2009), who reported a weighted mean age of 123.8 ± 0.2 Ma for 17 single crystals of sanidine, and plateau ages of 124.1 ± 0.2 and 124.1 ± 0.2 Ma for step-heated multigrain aliquots. While the data of Chang et al. (2009) are more consistent with the other $^{40}Ar/^{39}Ar$–$^{206}Pb/^{238}U$ data pairs than those of Swisher et al. (1999), there is no objective basis for excluding either data set *a priori*, except that Swisher et al. (1999) did not report relative isotope abundances corresponding to their plateau age, nor any information about the basis for the *J*-value or its contribution to the uncertainty budget. Accordingly, the data corresponding to the mean plateau age (124.1 ± 0.16 Ma) of Chang et al. (2009) are used for the present study. New U/Pb analyses of 6 annealed and chemically abraded zircon crystals from P1T-2 yielded a weighted mean $^{206}Pb/^{238}U$ age of 125.65 ± 0.17 Ma (MSWD 0.63).

PR94-7. This rock is a quartz-plagioclase-sanidine phyric rhyolite ash-flow tuff from the Arequita Fm., 4 km west of Lascano in southeastern Uruguay, where it appears to represent a late stage eruption of the voluminous Paraná-Etendeka flood volcanic province. $^{206}Pb/^{238}U$ (zircon) and $^{40}Ar/^{39}Ar$ data (sanidine) were obtained for this study. The ignimbrite is approximately 50 m thick, and is moderately to densely welded near its base. The sample was collected from ~20 m above the base. 16 individual zircons crystals from sample PR94-7 were subjected to either air abrasion or pretreated in ultrasonically agitated, hot HF aimed at minimizing the effects of Pb loss. 13 analyses yield a $^{206}Pb/^{238}U$ age of 133.06 ± 0.26 Ma (MSWD 1.0). An additional 6 zircons show distinctly older and/or discordant ages suggesting inheritance. Optically clear sanidine from the 20 to 40 mesh fraction (417–833 μm) of PR94-7 was separated by conventional methods and irradiated for 25 h in the OSTR reactor along with Fish Canyon sanidine (FCs) in three bracketing sample positions in an irradiation disk as described previously. Five single-crystal and one ten-crystal sample were analyzed by incremental heating to fusion using a CO_2 laser system with integrator lens. The $^{40}Ar^*/^{39}Ar_K$ value attributed to the standard (Table 3) is the arithmetic mean of three closely bracketing FCs aliquots. All of the experiments yielded well-defined age plateaux in mutual agreement within analytical errors, yielding MSWD = 0.5. Lower precision of the single-crystal experiments is due to the larger influence of background corrections on smaller argon yields.

NMB. The North Mountain basalt is part of the Central Atlantic Magmatic Province (CAMP). $^{206}Pb/^{238}U$ zircon data were reported by Schoene et al. (2006) and $^{40}Ar/^{39}Ar$ on plagioclase were reported by Jourdan et al. (2009). We use these data as reported in the original sources.

MSG-09. (45° 54.6′ N, 8° 54.6′ E) This bentonite occurs at the Anisian/Ladinian Grenzbitumenzone near Monte San Giorgio, Switzerland. $^{206}Pb/^{238}U$ (zircon) data and $^{40}Ar/^{39}Ar$ (sanidine) data from this bentonite were reported by Mundil et al. (2010).

SH-10. The sample is a bentonite equivalent to GS-1, for which $^{40}Ar/^{39}Ar$ on plagioclase were reported by Renne et al. (1995). New $^{40}Ar/^{39}Ar$ (plagioclase) data were obtained for this study by step-heating 3 multigrained aliquots that yielded indistinguishable plateau ages. Individual analysis of 13 crystals, combined with 38 previously reported by Renne et al. (1995), fail to reveal any xenocrystic contamination. The new results are combined with previous data as shown in Table 3. The FCs grains were loaded in the same well as the sample, in an irradiation disk similar to those depicted by Renne et al. (1998).

D3T. $^{206}Pb/^{238}U$ zircon data from this bentonite were reported by Mundil et al. (2004). This sample is equivalent to sample C-2, for which Renne et al. (1995) reported $^{40}Ar/^{39}Ar$ (sanidine) data. The data used herein are derived from these two sources.

SH-09. $^{206}Pb/^{238}U$ zircon data from this bentonite were reported by Mundil et al. (2004). New $^{40}Ar/^{39}Ar$ data (sanidine) were obtained for this study. Two multigrained aliquots were heated incrementally and yielded indistinguishable plateau ages, producing the data used herein (Table 3). Ten single crystal analyses yielded no evidence of xenocrysts. The FCs grains were loaded in the same well as the sample, in an irradiation disk similar to those depicted by Renne et al. (1998).

PD97-2. $^{40}Ar/^{39}Ar$ data (biotite) from this bentonite in the lower Quartermaster Fm. in Palo Duro State Park, Texas, were reported by Renne et al. (2001). New U–Pb data were obtained for this study. 7 out of 7 HF-leached zircons yielded a $^{206}Pb/^{238}U$ age of 253.02 ± 0.50 Ma (MSWD 1.2).

SH-27. $^{206}Pb/^{238}U$ zircon data from this bentonite were reported by Mundil et al. (2004). New $^{40}Ar/^{39}Ar$ data (sanidine) were obtained for this study. The sanidine crystals were sufficiently large that incremental heating of individual grains was possible, and nine such grains yielded indistinguishable plateau ages with MSWD of 0.44. The FCs grains were loaded in the same well as the sample, in an irradiation disk similar to those depicted by Renne et al. (1998).

SH-16. $^{206}Pb/^{238}U$ zircon data from this bentonite were reported by Mundil et al. (2004). New $^{40}Ar/^{39}Ar$ data (sanidine) were obtained for this study. A single multigrained aliquot was analyzed and yielded an age plateau comprising 100% of the ^{39}Ar released. Individual total fusion of 28 grains revealed no evidence of xenocrysts. The FCs grains were loaded in the same well as the sample, in an irradiation disk similar to those depicted by Renne et al. (1998).

SH-08. $^{206}Pb/^{238}U$ zircon data from this bentonite were reported by Mundil et al. (2004). New $^{40}Ar/^{39}Ar$ data (sanidine) were obtained for this study. Four multigrained aliquots were incrementally heated and yielded indistinguishable plateau ages with MSWD = 0.76. Individual total fusion of 23 grains revealed no evidence of xenocrysts. The FCs grains were loaded in the same well as the sample, in an irradiation disk similar to those depicted by Renne et al. (1998).

PaV. (36° 36.1′ S, 151° 36.9′ E) Sample PaV is from a ca. 100 m thick volcanic unit with quartz latite (toscanite) composition of Lower Carboniferous age exposed in a railway cut near Paterson (NSW, Australia) which is bracketed by clastic terrestrial sediments and used as a marker bed for the onset of the Kiaman magnetic superchron in Australia as well as the late Paleozoic Gondwana glaciation (Irving, 1966; Claoué-Long et al., 1995). U/Pb SHRIMP and ID-TIMS analyses by Claoué-Long et al. (1995) yielded ages of 330.1 ± 3.0 and 328.9 ± 4.2 Ma from the former and 327.7 ± 2.0 Ma from the latter technique. New $^{206}Pb/^{238}U$ (zircon) and $^{40}Ar/^{39}Ar$ (hornblende) data were obtained for this study. U/Pb analyses of annealed and chemically abraded zircons yield a $^{206}Pb/^{238}U$ age of 328.0 ± 0.5 Ma (MSWD 0.6) from six out of six crystals, in agreement with but more precise than the U/Pb ages from Claoué-Long et al. (1995). Five multigrain hornblende aliquots yielded $^{40}Ar/^{39}Ar$ plateaux with >90% of the ^{39}Ar released, yielding a weighted mean $^{40}Ar^*/^{39}Ar_K$ of 37.303 ± 0.032, MSWD = 2.0 and probability of fit = 0.094. To account for the excess scatter, the uncertainty was expanded by Students $t \times$ SQRT(MSWD) to give an uncertainty of $\sigma_R = 0.065$. The FCs grains were loaded in the same well as the sample, in an irradiation disk similar to those depicted by Renne et al. (1998).

DK-LQ. (37° 55.6′ N, 84° 55.9′ W). This sample is the Deicke bentonite collected at Lexington quarry, Kentucky. $^{40}Ar/^{39}Ar$ data for biotite single crystals were reported by Min et al. (2001), who employed a strict concordance criterion (plateaux comprising 100% of ^{39}Ar released; met by 9 of 11 crystals) to reject samples suspected of showing ^{39}Ar recoil redistribution effects from interlayered chlorite alteration present in some grains. New U/Pb zircon data were obtained for this study. Sixteen individual zircons were annealed and chemically abraded. Ten yielded a concordant cluster with a $^{206}Pb/^{238}U$ age of 454.59 ± 0.56 Ma (MSWD 1.8); five are distinctly older and clearly represent inherited grains; and 1 is resolvably younger and is inferred to reflect Pb-loss.

F-239. $^{207}Pb/^{206}Pb$ (zircon) and $^{40}Ar/^{39}Ar$ (anorthoclase) ages were reported by Min et al. (2000) for the Palisade Rhyolite, a densely welded ignimbrite of the North Shore volcanic group in Minnesota. Schoene et al. (2006) reported U/Pb (zircon) data for the same unit (sample #MS99-30), and their result is used herein. The $^{40}Ar/^{39}Ar$ results of Min et al. (2000) are adopted.

EGB-032. This sample is an unmetamorphosed hornblende–biotite dacite porphyry from the Eglab region of the Requibath massif, west Africa. U/Pb zircon data from this sample were reported by Schoene et al. (2006). New $^{40}Ar/^{39}Ar$ data (hornblende) were obtained from eleven single crystals, each yielding a plateau comprising >90% of the ^{39}Ar released, for this study. The individual plateau values of $^{40}Ar^*/^{39}Ar_K$ (F-values of Table 3) yield MSWD = 0.75. The FCs grains were loaded in the same well as the sample, in an irradiation disk similar to those depicted by Renne et al. (1998).

A.2. Calculation of ages and uncertainties

The $^{40}Ar/^{39}Ar$ age of an unknown based on the results presented herein can be calculated by solving Eq. (3) for τ_I, changing subscripts as appropriate, and substituting t_{unk} for τ_I.

$$t_{\text{unk}} = \frac{1}{(\lambda_{\text{tot}})} \ln\left[1 + \left(\frac{\lambda_{\text{tot}}}{\lambda_\varepsilon}\right) R^{\text{unk}}_{\text{FCs}} \cdot \kappa_{\text{FCs}}\right] \quad \text{(A.2.1)}$$

If the unknown is run with the FCs standard, R is as defined by Eq. (2). If another standard is used, the $^{40}Ar^*/^{39}Ar_K$ of the unknown must be referenced to FCs using the relationship:

$$R^{\text{unk}}_{\text{FCs}} \equiv R^{\text{unk}}_{\text{std1}} \cdot R^{\text{std1}}_{\text{std2}} \cdot \ldots \cdot R^{\text{stdn}}_{\text{FCs}} \quad \text{(A.2.2)}$$

and appropriate intercalibration factors as given by, e.g., Renne et al. (1998) for several widely used standards. Alternatively, R values relating the unknown to another standard may be used provided that a value of κ appropriate to that standard is also used. K–Ar ages may be simply computed by substituting (i) the measured $^{40}Ar^*/^{39}Ar_K$ for κ_{FCs} and (ii) a value of 1 for $R^{\text{unk}}_{\text{FCs}}$ in Eq. (A.2.1).

The linear error propagation formula given by Eq. (7) makes use of the following partial derivatives:

$$\frac{\partial t}{\partial \lambda_\varepsilon} = \frac{-1}{(\lambda_\varepsilon + \lambda_\beta)}\left[t + \frac{\lambda_\beta \kappa_{\text{FCs}} R}{(\lambda_\varepsilon^2 \kappa_{\text{FCs}} R + \lambda_\varepsilon \lambda_\beta \kappa_{\text{FCs}} R + \lambda_\varepsilon^2)}\right] \quad \text{(A.2.3)}$$

$$\frac{\partial t}{\partial \lambda_\beta} = \frac{1}{(\lambda_\varepsilon + \lambda_\beta)}\left[\frac{\kappa_{\text{FCs}} R}{(\lambda_\varepsilon \kappa_{\text{FCs}} R + \lambda_\beta \kappa_{\text{FCs}} R + \lambda_\varepsilon)} - t\right] \quad \text{(A.2.4)}$$

$$\frac{\partial t}{\partial \kappa_{\text{FCs}}} = \frac{R}{(\lambda_\varepsilon \kappa_{\text{FCs}} R + \lambda_\beta \kappa_{\text{FCs}} R + \lambda_\varepsilon)} \quad \text{(A.2.5)}$$

$$\frac{\partial t}{\partial R} = \frac{\kappa_{\text{FCs}}}{(\lambda_\varepsilon \kappa_{\text{FCs}} R + \lambda_\beta \kappa_{\text{FCs}} R + \lambda_\varepsilon)} \quad \text{(A.2.6)}$$

and the covariances given in Table 4b.

To illustrate the application of these equations, we detail the recalculation of the age of the Cretaceous/Tertiary boundary as given in Section 5.3. This is based on an age of 65.16 ± 0.04 Ma for the IrZ coal, as originally reported by Swisher et al. (1993) relative to an age of 27.84 Ma for FCs. We first calculate $R^{\text{IrZ}}_{\text{FCs}}$ using Eq. (2), using the value of λ_{tot} (5.543×10^{-10} a^{-1}) used in the original reference:

$$R^{\text{IrZ}}_{\text{FCs}} \equiv \frac{(^{40}Ar^*/^{39}Ar_K)_{\text{IrZ}}}{(^{40}Ar^*/^{39}Ar_K)_{\text{FCs}}} \equiv \frac{(e^{\lambda_{\text{tot}} t_{\text{IrZ}}} - 1)}{(e^{\lambda_{\text{tot}} t_{\text{FCs}}} - 1)} = \frac{(e^{5.543\times10^{-10}\cdot 6.516\times10^{7}} - 1)}{(e^{5.543\times10^{-10}\cdot 2.784\times10^{7}} - 1)} = 2.36496 \quad \text{(A.2.7)}$$

Application of Eq. (A.2.1) and the data in Table 4a yields an age of 66.236 Ma.

Uncertainty arising from the decay constants was neglected in the reported age, therefore by linear error propagation, the uncertainty in the value of $R^{\text{IrZ}}_{\text{FCs}}$ is given by:

$$\sigma_{R_{\text{IrZ}}} \equiv \frac{\lambda_{\text{tot}} e^{\lambda_{\text{tot}} \cdot t_{\text{IrZ}}}}{(e^{\lambda_{\text{tot}} \cdot t_{\text{FCs}}} - 1)} \sigma_{t_{\text{IrZ}}} = 0.00148 \text{ Ma} \quad \text{(A.2.8)}$$

Now the values of the partial derivatives can be computed from Eqs. A.2.3, A.2.4, A.2.5, A.2.6:

$$\frac{\partial t}{\partial \lambda_\varepsilon} = -1.1322 \times 10^{18} \text{ a}^2 \quad \text{(A.2.3)}$$

$$\frac{\partial t}{\partial \lambda_\beta} = -2.1670 \times 10^{15} \text{ a}^2 \quad \text{(A.2.4)}$$

$$\frac{\partial t}{\partial \kappa_{\text{FCs}}} = 3.9612 \times 10^{10} \ a \quad \text{(A.2.5)}$$

$$\frac{\partial t}{\partial R} = 2.7499 \times 10^{7} \ a \quad \text{(A.2.6)}$$

Application of these values, and the covariances given in Table 4b, to Eq. (7) yields an age uncertainty of $\sigma_{t_{\text{IrZ}}} = 0.041$ Ma. As noted in the text however, linear error propagation is somewhat inaccurate for very precise R-values such as in this case, where $\sigma_{R_{\text{IrZ}}}/R_{\text{IrZ}} = 0.06\%$. Instead, Monte Carlo simulation is preferred and in this case yields an uncertainty of ± 0.060 Ma as shown in Table 5, based on the distributions given in EA-3.

An Excel spreadsheet which performs age calculations and both linear and Monte Carlo error estimation, based on the results presented herein, is available on request from the corresponding author (P.R.R.).

APPENDIX B. SUPPLEMENTARY DATA

Supplementary data associated with this article can be found, in the online version, at doi:10.1016/j.gca.2010.06.017.

REFERENCES

Aguilar J. P., Clauzon G., deHerve A. D., Maluski H., Michaux J. and Welcomme J. L. (1996) The MN3 fossil mammal-bearing locality of Beaulieu (France): biochronology, radiometric dating, and lower age limit of the Early Neogene renewal of the mammalian fauna in Europe. *Newsl. Stratigr.* **34**, 177–191.

Bachman O., Oberli F., Dungan M. A., Meier M., Mundil R. and Fischer H. (2007) $^{40}Ar/^{39}Ar$ and U–Pb dating of the Fish Canyon magmatic system, San Juan Volcanic Field, Colorado: evidence for an extended crystallization history. *Chem. Geol.* **236**, 134–166.

Bacon C. R. and Lowenstern J. B. (2005) Late Pleistocene granodiorite source for recycled zircon and phenocrysts in rhyodacite lava at Crater Lake, Oregon. *Earth Planet. Sci. Lett.* **233**, 277–293.

Baksi A. K., Archibald D. A. and Farrar E. (1996) Intercalibration of $^{40}Ar/^{39}Ar$ dating standards. *Chem. Geol.* **129**, 307–324.

Beckinsale R. D. and Gale N. H. (1969) A reappraisal of the decay constants and branching ratio of ^{40}K. *Earth Planet. Sci. Lett.* **6**, 289–294.

Begemann F., Ludwig K. R., Lugmair G. W., Min K., Nyquist L. E., Patchett P. J., Renne P. R., Shih C.-Y., Villa I. M. and Walker R. J. (2001) Call for an improved set of decay constants for geochronological use. *Geochim. Cosmochim. Acta* **65**, 111–121.

Black L. P., Kamo S. L., Allen C. M., Davis D. W., Aleinikoff J. N., Valley J. W., Mundil R., Campbell I. H., Korsch R. J., Williams I. S. and Foudoulis C. (2004) Improved $^{206}Pb/^{238}U$ microprobe geochronology by the monitoring of a trace-element-related matrix effect; SHRIMP, ID-TIMS, ELA-ICP-MS and oxygen isotope documentation for a series of zircon standards. *Chem. Geol.* **205**, 115–140.

Bukowinski M. S. T. (1979) Theoretical estimate of compressional changes of decay constant of ^{40}K. *Geophys. Res. Lett.* **6**, 697–699.

Cande S. C. and Kent D. V. (1995) Revised calibration of the geomagnetic polarity timescale for the Late Cretaceous and Cenozoic. *J. Geophys. Res. Solid Earth* **100**, 6093–6095.

Chang S.-C., Zhang H., Renne P. R. and Fang Y. (2009) High-precision $^{40}Ar/^{39}Ar$ age of the Jehol Biota. *Paleogeogr. Paleoecol. Paleoclimatol.* **280**, 94–104.

Channell J. E. T., Mazaud A., Sullivan P., Turner S. and Raymo M. E. (2002) Geomagnetic excursions and paleointensities in the Matuyama Chron at Ocean Drilling Program Sites 983 and 984 (Iceland Basin). *J. Geophys. Res.* **107**(6).

Channell J. E. T., Curtis J. H. and Flower B. P. (2004) The Matuyama–Brunhes boundary interval (500–900 ka) in North Atlantic drift sediments. *Geophys. J. Int.* **158**, 489–505.

Claoué-Long J. C., Compston W., Roberts J. and Fanning C. M. (1995) Two Carboniferous ages: a comparison of SHRIMP zircon dating with conventional zircon ages and $^{40}Ar/^{39}Ar$ analysis. In *Geochronology, Time Scales and Stratigraphic Correlation*, vol. 54 (eds. W. Berggren, D. Kent, M. Aubry and J. Hardenbol). SEPM Special Publication, pp. 1–22.

Coe R. S., Singer B. S., Pringle M. S. and Zhao X. X. (2004) Matuyama–Brunhes reversal and Kamikatsura event on Maui: paleomagnetic directions, $^{40}Ar/^{39}Ar$ ages and implications. *Earth Planet. Sci. Lett.* **222**, 667–684.

Crowley J. L., Schoene B. and Bowring S. A. (2007) U–Pb dating of zircon in the Bishop Tuff at the millennial scale. *Geology* **35**, 1123–1126.

Dazé A., Lee J. K. W. and Villeneuve M. (2003) An intercalibration study of the Fish Canyon sanidine and biotite $^{40}Ar/^{39}Ar$ standards and some comments on the age of the Fish Canyon Tuff. *Chem. Geol.* **199**, 111–127.

Dodson M. H. (1973) Closure temperature in cooling geochronological and petrological systems. *Contrib. Mineral. Petrol.* **40**, 259–274.

Endt P. M. and Van der Leun C. (1973) Energy levels of A = 21–44 nuclei (V). *Nucl. Phys.* **A214**, 1–625.

Fleck R. J., Sutter J. F. and Elliot D. H. (1977) Interpretation of discordant $^{40}Ar/^{39}Ar$ age spectra of Mesozoic tholeiites from Antarctica. *Geochim. Cosmochim. Acta* **41**, 15–32.

Garner E. L., Murphy T. J., Gramlich J. W., Paulsen P. J. and Barnes I. L. (1975) Absolute isotopic abundance ratios and the atomic weight of a reference sample of potassium. *J. Res. Natl. Bur. Stand.* **79A**, 713–725.

Gradstein F., Ogg J. and Smith A. (2004) *A Geologic Time Scale 2004*. University Press, Cambridge, p. 611.

Grau Malonda A. and Grau Carles A. (2002) Half-life determination of ^{40}K by LSC. *Appl. Radiat. Isot.* **56**, 153–156.

Hilgen F. J., Krijgsman W. and Wijbrans J. R. (1997) Direct comparison of astronomical and $^{40}Ar/^{39}Ar$ ages of ash beds: potential implications for the age of mineral dating standards. *Geophys. Res. Lett.* **24**, 2043–2046.

Hurford A. J. and Hammerschmidt K. (1985) $^{40}Ar/^{39}Ar$ and K/Ar Dating of the Bishop and Fish Canyon Tuffs: calibration of ages for fission-track dating standards. *Chem. Geol.* **58**, 23–32.

Irving E. (1966) Paleomagnetism of some Carboniferous rocks from New South Wales and its relation to geological events. *J. Geophys. Res.* **71**, 6025–6051.

Jaffey A. H., Flynn K. F., Glendenin L. E., Bentley W. C. and Essling A. M. (1971) Precision measurement of half-lives and specific activities of ^{235}U and ^{238}U. *Phys. Rev.* **C4**, 1889–1906.

Jourdan F. and Renne P. R. (2007) Age calibration of the Fish Canyon sanidine $^{40}Ar/^{39}Ar$ dating standard using primary K–Ar standards. *Geochim. Cosmochim. Acta* **71**, 387–402.

Jourdan F., Marzoli A., Bertrand H., Cirilli S., Tanner L. H., Kontak D. J., McHone G., Renne P. R. and Bellieni G. (2009) $^{40}Ar/^{39}Ar$ ages of CAMP in North America: Implications for the Triassic–Jurassic boundary and the ^{40}K decay constant bias. *Lithos* **110**, 167–180.

Kossert K. and Günther E. (2004) LSC measurements of the half-life of ^{40}K. *Appl. Radiat. Isot.* **60**, 459–464.

Kuiper K. F., Deino A., Hilgen F. J., Krijgsman W., Renne P. R. and Wijbrans J. R. (2008) Synchronizing the rock clocks of Earth history. *Science* **320**, 500–504.

Kwon J., Min K., Bickel P. and Renne P. R. (2002) Statistical methods for jointly estimating decay constant of ^{40}K and age of a dating standard. *Math. Geol.* **34**, 457–474.

Lagarias J. C., Reeds J. A., Wright M. H. and Wright P. E. (1998) Convergence properties of the Nelder–Meade Simplex method in low dimensions. *SIAM J. Optim.* **9**, 112–147.

Lanphere M. A. and Baadsgaard H. (2001) Precise K–Ar, $^{40}Ar/^{39}Ar$, Rb–Sr and U/Pb mineral ages from the 27.5 Ma Fish Canyon Tuff reference standard. *Chem. Geol.* **175**, 653–671.

Lanphere M. A. and Dalrymple G. B. (2000) First principles calibration of ^{38}Ar tracers; implications for the ages of $^{40}Ar/^{39}Ar$ fluence monitors. *U.S. Geological Survey Professional Paper* **1621**, p. 10.).

Lourens L., Hilgen F., Shackleton N. J., Laskar J. and Wilson J. (2004) Appendix 2. Orbital tuning calibrations and conversions for the Neogene Period. In *A Geologic Time Scale 2004* (eds. F. M. Gradstein, J. G. Ogg and A. G. Smith). Cambridge University Press, pp. 469–471.

Luck J. M., Birck J. L. and Allègre C. J. (1980) ^{187}Re-^{187}Os systematics in meteorites; early chronology of the solar system and age of the Galaxy. *Nature* **283**, 256–259.

Ludwig K. R. (1998) On the treatment of concordant uranium-lead ages. *Geochim. Cosmochim. Acta* **62**, 665–676.

Ludwig K. R. (2000) Decay constant errors in U–Pb concordia-intercept ages. *Chem. Geol.* **166**, 315–318.

Mattinson J. M. (1987) U–Pb ages of zircons – a basic examination of error propagation. *Chem. Geol.* **66**, 151–162.

Mattinson J. M. (2005) Zircon U–Pb chemical abrasion ("CA-TIMS") method: Combined annealing and multi-step partial dissolution analysis for improved precision and accuracy of zircon ages. *Chem. Geol.* **220**, 47–66.

Mattinson J. M. (in press) Analysis of the relative decay constants of ^{235}U and ^{238}U by Multi-step CA-TIMS Measurements of Closed-System Natural Zircon Samples. *Chem. Geol.* doi:10.1016/j.chemgeo.2010.05.007.

McIntyre G. A., Brooks C., Compston W. and Turek A. (1966) The statistical assessment of Rb/Sr isochrons. *J. Geophys. Res.* **71**, 5459–5468.

Min K., Mundil R., Renne P. R. and Ludwig K. R. (2000) A test for systematic errors in $^{40}Ar/^{39}Ar$ geochronology through comparison with U–Pb analysis of a 1.1 Ga rhyolite. *Geochim. Cosmochim. Acta* **64**, 73–98.

Min K., Renne P. R. and Huff W. D. (2001) $^{40}Ar/^{39}Ar$ dating of Ordovician K-bentonites in Laurentia and Baltoscandia. *Earth Planet. Sci. Lett.* **185**, 121–134.

Minster J.-F., Birck J. L. and Allègre C. J. (1982) Absolute age of formation of chondrites studied by the ^{87}Rb–^{87}Sr method. *Nature* **300**, 414–419.

Mundil R., Metcalfe I., Ludwig K. R., Renne P. R., Oberli F. and Nicoll R. S. (2001) Timing of the Permian–Triassic biotic crisis: implications for new zircon U/Pb age data (and their limitations). *Earth Planet. Sci. Lett.* **187**, 133–147.

Mundil R., Ludwig K. R., Metcalf I. and Renne P. R. (2004) Age and timing of the end Permian mass extinction: U–Pb geochronology of closed system zircons. *Science* **305**, 1760–1763.

Mundil R., Palfy J., Renne P. R. and Brack P. (2010) The Triassic time scale: new constraints and a review of geochronological data. In *The Triassic Timescale*, vol. 334 (ed. S. G. Lucas). Geological Society, London, pp. 41–60, Special Publications.

Nomade S., Renne P. R., Vogel N., Deino A. L., Sharp W. D., Becker T. A., Jaouni A. R. and Mundil R. (2005) Alder Creek Sanidine (ACs-2): a quaternary $^{40}Ar/^{39}Ar$ dating standard tied to the Cobb Mountain geomagnetic event. *Chem. Geol.* **218**, 319–342.

Norman E. B., Rech G. A., Browne E., Larimer R. M., Dragowsky M. R., Chan Y. D., Isaac M. C. P., McDonald R. J. and Smith A. R. (2001) Influence of physical and chemical environments on the decay rates of ^{7}Be and ^{40}K. *Phys. Lett. B* **519**, 15–22.

Palfy J., Mundil R., Renne P. R., Bernor R. L., Kordos L. and Gasparik M. (2007) M., U–Pb and $^{40}Ar/^{39}Ar$ dating of the Miocene fossil track site at Ipolytarnóc (Hungary) and its implications. *Earth Planet. Sci. Lett.* **258**, 160–174.

Patchett P. J. and Tatsumoto M. (1980) Lu–Hf total-rock isochron for the eucrite meteorites. *Nature* **288**, 571–574.

Renne P. R. and Min K. (1998) $^{40}Ar/^{39}Ar$ dating of the 79 AD eruption of Vesuvius: An ab initio basis for improved accuracy in $^{40}Ar/^{39}Ar$ geochronology. *Mineral. Mag.* **62A**, 1255–1256.

Renne P. R., Deino A. L., Walter R. C., Turrin B. D., Swisher C. C., Becker T. A., Curtis G. H., Sharp W. D. and Jaouni A.-R. (1994) Intercalibration of astronomical and radioisotopic time. *Geology* **22**, 783–786.

Renne P. R., Zichao Z., Richards M. A., Black M. T. and Basu A. R. (1995) Synchrony and causal relations between Permian–Triassic boundary crises and siberian flood volcanism. *Science* **269**, 1413.

Renne P. R., Sharp W. D., Deino A. L., Orsi G. and Civetta L. (1997) $^{40}Ar/^{39}Ar$ Dating into the historical realm: calibration against pliny the younger. *Science* **277**, 1279–1280.

Renne P. R., Swisher C. C., Deino A. L., Karner D. B., Owens T. and DePaolo D. J. (1998) Intercalibration of standards, absolute ages and uncertainties in $^{40}Ar/^{39}Ar$ dating. *Chem. Geol. (Isotope Geoscience Section)* **145**, 117–152.

Renne P. R., Sharp W. D., Montañez I. P., Becker T. A. and Zierenberg R. A. (2001) $^{40}Ar/^{39}Ar$ dating of Late Permian evaporites, southeastern New Mexico, USA. *Earth Planet. Sci. Lett.* **193**, 539–547.

Sarna-Wojcicki A. M., Pringle M. S. and Wijbrans J. (2000) New $^{40}Ar/^{39}Ar$ age of the Bishop Tuff from multiple sites and sediment rate calibration for the Matuyama–Brunhes boundary. *J. Geophys. Res.* **105**, 21,431–21,443.

Schmitz M. D. and Bowring S. A. (2001) U–Pb zircon and titanite systematics of the Fish Canyon Tuff: an assessment of high-precision U–Pb geochronology and its application to young volcanic rocks. *Geochim. Cosmochim. Acta* **65**, 2571–2578.

Schoene B., Crowley J. L., Condon D. J., Schmitz M. D. and Bowring S. A. (2006) Reassessing the uranium decay constants for geochronology using ID-TIMS U/Pb data. *Geochim. Cosmochim. Acta* **70**, 426–445.

Schön R., Winkler G. and Kutschera W. (2004) A critical review of experimental data for the half-lives of the uranium isotopes ^{238}U and ^{235}U. *Appl. Radiat. Isot.* **60**, 263–273.

Simon J. I. and Reid M. R. (2005) The pace of rhyolite differentiation and storage in an "archetypical" silicic magma system, Long Valley, California. *Earth Planet. Sci. Lett.* **235**, 123–140.

Simon J. I., Renne P. R. and Mundil R. (2008) Implications of pre-eruptive magmatic histories of zircons for U–Pb geochronology of silicic extrusions. *Earth Planet. Sci. Lett.* **266**, 182–194.

Smith M. E., Chamberlain K. R., Singer B. S. and Carroll A. R. (2010) Eocene clocks agree: coeval $^{40}Ar/^{39}Ar$, U–Pb and astronomical ages from the Green River Formation. *Geology* **38**, 527–530.

Spell T. L. and McDougall I. (2003) Characterization and calibration of $^{40}Ar/^{39}Ar$ dating standards. *Chem. Geol.* **198**, 189–211.

Steiger R. H. and Jäger E. (1977) Subcommission on geochronology: convention on the use of decay constants in geo- and cosmochronology. *Earth Planet. Sci. Lett.* **6**, 359–362.

Steven T. A., Mehnert H. H. and Obradovich J. D. (1967) Age of volcanic activity in the San Juan Mountains, Colorado. *U.S. Geol. Surv. Prof. Pap.* **575D**, D47–D55.

Swisher C. C., Dingus L. and Butler R. F. (1993) $^{40}Ar/^{39}Ar$ Dating and magnetostratigraphic correlation of the terrestrial cretaceous-paleogene boundary and puercan mammal age, Hell Creek – Tullock Formations, Eastern Montana. *Can. J. Earth Sci.* **30**, 1981–1996.

Swisher C. C., Wang Y. Q., Wang X. L., Xu X. and Wang Y. (1999) Cretaceous age for the feathered dinosaurs of Liaoning, China. *Nature* **400**, 58–61.

Villeneuve M., Sandeman H. A. and Davis W. A. (2000) A method for intercalibration of U–Th–Pb and ^{40}Ar–^{39}Ar ages in the Phanerozoic. *Geochim. Cosmochim. Acta* **64**, 4017–4030.

Wetherill G. W., Wasserburg G. J., Aldrich L. T., Tilton G. R. and Hayden R. J. (1956) Decay Constants of ^{40}K as determined from the radiogenic argon content of potassium minerals. *Phys. Rev.* **103**, 987–989.

Associate editor: Peter W. Reiners